MEMS ultrasound for active implantable devices

Marta Saccher

TU Delft

MEMS ultrasound for active implantable devices

By

Marta Saccher

in partial fulfilment of the requirements for the degree of

Master of Science

in Biomedical Engineering

at the Delft University of Technology,

to be defended publicly on Friday September 20, 2019 at 10:00 AM.

Supervisors:	Prof. dr. ir. R. Dekker	
	Ir. S. Kawasaki	
Thesis committee:	Prof. dr. ir. R. Dekker,	TU Delft
	Prof. dr. P.J. French,	TU Delft
	Dr. V. Giagka,	TU Delft
	Prof. dr. P.G. Steeneken,	TU Delft
	Dr. G. van Woerden,	Erasmus MC

TU Delft

Abstract

During the past decade, Implantable biomedical devices have emerged as an efficient treatment for neurological disorders. Among them, low-intensity focused ultrasound (LIFU) has recently gained interest due to its focusing ability, depth of penetration and reversible effects. Although the exact biophysical mechanism that leads to the interaction between ultrasound and neurons is not clear yet, many successful applications have been reported both *in vitro* and *in vivo* in animals, raising prospects for clinical applications. Nevertheless, treatments were mainly delivered transcranially due to the lack of implantable technologies, constraining the frequency range to below 1 MHz. Thanks to the development of biocompatible capacitive micromachined ultrasound transducers (CMUTs), ultrasound has become implantable, opening the way for high frequency ultrasound neuromodulation.

In addition, implantable biomedical devices are becoming smaller and smaller, requiring their power supply to follow this trend. Batteries can be a limiting factor for their miniaturisation and other powering methods have been investigated. Among them, ultrasound as a means to wirelessly transfer power represents the best trade-off between the amount of available power, implanted receiver size, and depth of penetration. Also in this case, biocompatible CMUTs could be used as transducers to power an implanted device. Yet they require a DC bias source in the order of tens of volts which is not practical for an implanted device.

In this thesis the application of ultrasound for implantable biomedical devices is investigated. First, the modulation of the excitability of *in vitro* mice hippocampal brain slices (normal and epileptic) using high frequency sonication protocols is explored. Secondly, wireless power transfer using CMUT devices with charges trapped in the dielectric which do not require a DC bias voltage is investigated.

The results indicate that high frequency ultrasound clearly affects the excitability of neurons, having an excitatory effect when delivered using a 5 MHz continuous wave sonication protocol, while it inhibits the neurons when they are exposed to pulsed wave ultrasound at 13 MHz. The intensities used were in line or much lower compared to values used by other groups of researchers. In addition, ultrasound power transfer with an efficiency higher than 48% was achieved using CMUT devices with charges permanently trapped in their Al_2O_3 layer. This efficiency was in line with values obtained by other groups using piezoelectric transducers.

Based on these results, it is clear that ultrasound, specifically using implantable CMUT devices, has a great potential to be used in bioelectronic medicine applications for both the treatment of neurological disorders as well as a means of power transfer.

Keywords: ultrasound, neuromodulation, power transfer, CMUT

Acknowledgments

I would like to thank several people for their contribution to this Master Thesis.

Ronald, for giving me the possibility to take part of this research. Your enthusiasm and your interest in the results I was showing to you have been really motivating. Thank you for teaching me how to make bitterballen and, although we don't agree on which is the best weather, I hope our paths will cross again in the future.

Shin, for believing in my ideas and capabilities. Thank you for asking me a lot of questions, they have been really precious to understand my results and look 'beyond the data'. Your door has been always open whenever I had something to ask and I really enjoyed the discussions that we had, not only about our research topics.

Jian, for being always optimistic about my future and for our gossip. It was so nice to laugh with you! Lambert, for the precious advices you gave me and for tolerating me in your office when I was discussing with Shin. I still smile when I think we found out to be birth mates.

All the intern community and, in particular, the 'wine Wednesday and lasagne'. Thank you for making my life at Philips and outside colourful and crazy! I had so much fun and I hope we will keep in touch and meet again somewhere around the word in the future!

Geeske and Martina. Thank you for your enthusiasm and for believing in our experiment and giving us a second chance, although you were really busy! Thank you also for opening the doors to the biology world and sharing your extensive knowledge.

Peter Dirksen, Peter Blanken, Bert of het Veld and Peter Loebl for their advices and the discussions that we had. They have been really helpful.

Mark de Haas, for the measurements of the CMUT impedance and the pressure profile of the ultrasound transducers. Although you are often really busy, you always found a spot in your agenda to measure my devices.

All the other researchers at Philips which helped me in other different circumstances. Thank you for your valuable advices.

Martina and Paolo. You are the best friends I could ask for! Thank you for the laughter and the craziness we share. Thank you for the support and our infinite Skype calls. I miss you so much!

To all my friends from all over the world. Thank you for opening my mind with your stories, habits and costumes. Thank you for making my Dutch years so nice and enriching.

To my parents. Thank you for always supporting me! Without you this would have never been possible. *Grazie mamma e papà!* Thank you for all the love you gave me and for teaching me to be always curious and to never give up. You taught me how to make do with what I have and to be proud of it. You have always been there in every moment of my life and I am happy I could make you prod!

Contents

List of figures

List of tables

1 Introduction

Ultrasound refers to acoustic waves in the range of frequencies above 20kHz. It is used in many applications which require the detection of objects or the measurement of distances. In medicine, it is mainly used to visualise structures inside the body in a non-invasive way, for therapeutic purposes such as thermal ablation of the soft tissues, physiotherapies of the muscular conditions, and lithotripsy of the kidney stones [1].

Ultrasound is generated by ultrasound transducers, which convert energy from the electrical to the mechanical domain and vice versa. They can be either piezoelectric transducers or capacitive micromachined ultrasound transducers (CMUT). While the former relies on the material's intrinsic piezoelectric properties, the latter are based on Micro-Electro-Mechanical Systems (MEMS) technology. Among the different piezoelectric materials, PZT (lead zirconate titanate) is most commonly used, however it contains lead and is therefore not biocompatible. On the other side, thanks to the advancements in both fabrication technology and materials science, CMUT devices can be made biocompatible, and could therefore be implanted in the body [2].

This, together with their ease of fabrication compared to piezoelectric transducers, opens the way for their use in many other biomedical applications. In this thesis, the effects of high frequency ultrasound on the excitability of the nervous system are investigated in order to determine the feasibility of this neuromodulation technique to potentially encourage the research on the fabrication of CMUT devices for this application. As a second application, the use of CMUT devices as an implantable ultrasound transducer to wirelessly power implantable bioelectronics is explored.

The thesis is therefore divided in two parts. **In the first part**, including chapters from 2 to 7, the ability of ultrasound to modulate the spontaneous activity of *in vitro* mice hippocampi is presented. This was done by designing an experimental setup and various sonication protocols to be tested on the cell preparations. **The second part**, including Chapters from 8 to 12, presents the calculation of the power transfer efficiency of capacitive micromachined ultrasound devices with charges trapped into the dielectric. A general conclusion, presenting the main achievements, is provided at the end of the thesis, in Chapter 13.

ULTRASOUND NEUROMODULATION OF *in vitro* BRAIN CELLS

2 Introduction

Neurological disorders are disorders of the nervous system of which the most common are epilepsy, Parkinson's disease, motor neuron diseases, migraine and strokes. They affect brain, spinal cord, nerves and muscles, and in 2015 these diseases were counted as 16.8% of the world's disease burden [3], [4] with an expectancy to grow in both low and high-income countries over the next decades [5].

The most common treatments to neurological disorders are pharmacological interventions and surgical treatments. Sometimes they are not effective in treating the disease due to the development of drug dependencies, lack of spatial specificity or incompatibility with surgery. However, in the past few decades other treatment methods have been developed which include deep brain stimulation (DBS), transcranial magnetic stimulation (TMS), vagus nerve stimulation (VNS) and infrared radiation [6]. Like pharmacological treatments, TMS and infrared lack spatial specificity, but they have the benefit of being non-invasive [7]. DBS can reach high specificity but it requires surgery and implantation of the stimulating electrodes deep into the brain which may cause inflammation, bleeding and cell death [8].

It is therefore evident that solutions that are both non- or less-invasive and with higher spatial specificity need to be investigated. The most promising candidate is represented by ultrasound whose capability of modulating the nervous system was discovered almost one century ago by Harvey who observed the twitching of a frog sciatic nerve during irradiation with ultrasound [9]. In the last few years the number of studies on ultrasound effects on peripheral nerves, receptors and brain excitability has increased, and it has been found that low-intensity focused ultrasound (LIFU) waves can reversibly elicit or suppress neuronal activity [10]. In addition, focused ultrasound can reach submillimetre precision, which makes it ideal for precise neuromodulation [11].

2.1 Biophysics of ultrasound

The interaction between acoustic waves and biological tissues depends on the tissue properties, ultrasound beam configuration and exposure parameters. In liquid media, such as water or idealised soft tissues, ultrasound waves can only propagate longitudinally, meaning that the particles inside the media moves back and forth with respect to the direction of propagation of the acoustic wave [6], [12]. They are generated by an ultrasound transducer that can output a plane wave, in case of unfocused devices, or concentrate the acoustic energy in a specific location, the focus point, in case of focused devices. The focusing effect is one of the most important characteristics of ultrasound and can be achieved by designing specific lenses for the transducer or with beamforming techniques.

The type of medium determines also the speed of propagation of the acoustic waves, which in water-based media, has an average velocity of 1500 m/s. This value dramatically increases in hard tissues like bones. The sound velocity within the medium *c,* influences the characteristic acoustic impedance (Z), defined as $Z = \pm\rho c$ where ρ represents the density of the medium. The additional sign, determines whether the wave is travelling forward (+) or backward (-) [12]. Furthermore, the acoustic impedance distinguishes a certain medium, and it may be different in two adjacent structures. The type of medium is also responsible for the amount of energy that is attenuated by the medium. The attenuation coefficient (α) is described by the relation $\alpha(f) = \alpha_0 f^b$ where α_0 and b are parameters whose values depend on the tissue, while f is the frequency [6]. α is measured in $dB\ cm^{-1}MHz^{-1}$, therefore the penetration of the

acoustic wave in the tissue is inversely proportional to the frequency. This is described by an exponential that models the decrease of the ultrasound wave intensity along its path, expressed by the relation:

$$I = I_0 \cdot e^{-\alpha x} \tag{2.1}$$

Where I_0 is the intensity at $x = 0$. The energy lost is being absorbed by the tissue in the beam path and if the rate of heat production is higher than the rate of heat removal, the temperature of the medium increases. As the temperature increases, the rate of biochemical reactions also rises, and if the temperature is too high, proteins can denature [12]. This mechanism is used, for example, in ultrasound tissue ablation therapies. However, in case of neuromodulation, temperature increase should be avoided to prevent the formation of lesions. The thermal index (TI) is used to quantify the temperature elevation:

$$TI = \frac{I_0}{I_{DEG}} \tag{2.2}$$

where I_0 is the acoustic power at the depth of interest and I_{DEG} is the estimated power necessary to raise the tissue equilibrium temperature by 1°C [12]. Depending on the type of tissue exposed to ultrasound, three different thermal indices are defined: thermal index for soft tissue (TIS), thermal index for bone at focus (TIB) and thermal index for bone at the surface (TIC) [13].

Besides thermal effects, ultrasound can interact with tissues mechanically via cavitation or acoustic radiation force. Cavitation is the development of microscopic bubbles in an acoustic field when subjected to high negative pressures. Two types of cavitation can be defined: inertial cavitation and stable cavitation. The former can cause the bubble to collapse, imploding or exploding, and depending on the violence of the effect it could lead to the formation of free radicals [14], but also to tissue destruction. This principle is used for the fragmentation of kidney stones. On the other hand, stable cavitation does not produce damage and can be safely used to induce changes in the conductance of the cell membrane [15]. The second mechanism, acoustic radiation force, is the development of a mechanical force proportional to the intensity of the acoustic wave which displaces the sonicated medium [16]. To estimate the strength of the mechanical interaction, the mechanical index (MI) is used:

$$MI = max\left\{\frac{p_{neg}}{\sqrt{f}}\right\} \tag{2.3}$$

where p_{neg} is the peak negative pressure in MPa and f the sonication frequency in MHz.

While High Intensity Focused Ultrasound (HIFU), is typically used for the ablation or fractionation of soft tissue [17], Low Intensity Focused Ultrasound (LIFU) has been found to excite and inhibit neural tissue with intensities similar to the ones used in ultrasound imaging. However, safety limits for the use of ultrasound for neuromodulation have not yet been defined. Therefore, the maximum ultrasound output levels used for imaging applications are used as a reference for neural stimulation. The maximum allowed intensity, mechanical and thermal indices are summarised in Table 1.

Table 1 Safety limits for ultrasound neuromodulation [17]

TI	≤ 6
MI	≤ 1.9
I_{spta}	≤ 720 mW/cm^2
I_{sppa}	≤ 190 W/cm^2

2.2 Cellular mechanisms behind ultrasound induced neuromodulation

The principle behind ultrasound neuromodulation is the modification of the signalling between neurons by which by the brain receives sensory information and issues motor commands. Neurons, like other cells in the body, have a separation of charge across their membrane, responsible for the resting potential. Electrical perturbations, such as action potentials or electrical stimulation, can cause the secretion of neurotransmitters at chemical synapses. They will link to specific receptors of neighbouring neurons and activate or deactivate ionic channels, causing an ionic current through the membrane and modifying the potential across it. However, other than chemically-regulated channels, the ionic flow through the membrane of the neurons is determined also by channels regulated mechanically or thermally with which ultrasound waves are thought to interact. There are four main theories that attempt to explain the mechanism behind the generation of action potentials during US exposure.

The first one is the direct mechanical alteration of the mechanosensitive ion channels within the cellular membrane due to US. These are the voltage-gated ion channels (sodium, potassium and calcium channels) which possess mechanosensitive properties. The acoustic wave displaces the cellular membrane in which the channels reside, activating them and causing the generation of an action potential [18], [19].

The second mechanism is the effect of acoustic cavitation which could create nanobubbles inside the lipid bilayer of the cell membrane. Ultrasound causes their expansion and contraction consequently modifying the conformation of the membrane. This could first activate mechanosensitive channels and, if the applied pressure is high enough to cause their collapse, pores or other similar openings could be formed. As a consequence, the permeability of the membrane will change, altering the ionic currents, therefore the process of action potential generation [20].

The concept of acoustic cavitation is also the starting point for the formulation of the third hypothetical mechanism. Conformational changes of the cell membrane result in the variation of its electrical properties. Rapid oscillations of the two layers of the cell membrane are hypothesized to result in a variation of its capacitance (C), giving rise to hyperpolarising currents proportional to the membrane potential and the capacitance variation ($\propto V \cdot dC/dt$) [21].

The fourth mechanism is related to the thermal effects of ultrasound. It has been shown that the increase of temperature can disrupt the synaptic contacts , therefore being more likely to contribute to the inhibition of the neural activity [22].

However, what is the exact molecular mechanism leading the interaction between ultrasound waves and neural tissue is not clear yet and more likely it involves a combination of multiple factors, including also the sonication protocol.

2.3 Ultrasound parameters for the modulation of the nervous system

Ultrasound neuromodulation protocols are distinguished by the transmitting mode of the acoustic waves, which could be continuous wave (CW) or pulsed wave (PW). In continuous wave mode, the acoustic wave is transmitted for the entire duration of the treatment, while in PW mode, the acoustic wave is *on* only for a short duration, named tone burst duration (TBD), during which a certain number of wave cycles occur, and after which on *off* period follows. The rhythmic alternation of the *on* and *off* period has usually a constant frequency, named pulse repetition frequency (PRF), and it is repeated for a defined time period which is the treatment time (Figure 1.A).

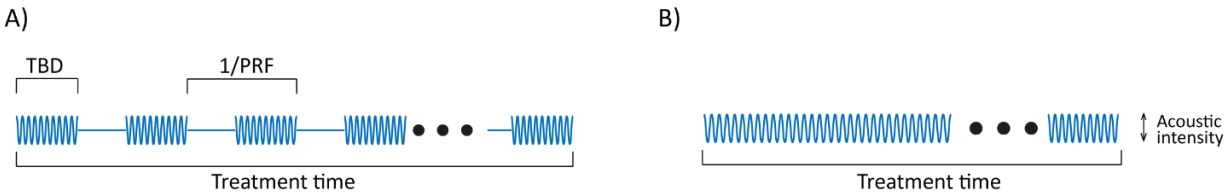

Figure 1 Graphical representation of the sonication parameters with respect to the protocol. A) Pulsed wave. B) Continuous wave.

Ultrasound waves are generated by an ultrasound transducer which outputs an acoustic beam with an intensity depending on its driving voltage. Two definitions of intensity are being used. Spatial-peak temporal-averaged intensity (I_{SPTA}), which is the intensity averaged over the treatment time, and spatial-peak pulse-averaged intensity (I_{SPPA}), which is the average ultrasound intensity in each tone-burst. Further details on their mathematical formulation can be found in Appendix A.

The effects of ultrasound neuromodulation have been demonstrated by experiments in both *in vitro* and *in vivo*, mainly on small size animals, highlighting that the outcome of the experiments depends on the careful tuning of the different parameters presented above. Both excitation and inhibition of the neural activity can be achieved, although there is still no agreement on the optimal combination of US parameters to achieve a specific neuromodulatory effect.

The acoustic beam must deliver a sufficient amount of energy to the target tissue in order to alter its excitability, but it has to remain below the safety limits to avoid permanent damage. The intensity of an US beam attenuates exponentially with the propagation in the tissue due to its dependence on the sonication frequency. Therefore, the higher the frequency, the higher is the intensity required to obtain a neuromodulatory effect. This can be seen in Figure 2.A where the relationship between intensity and frequency is depicted. The values were obtained from the analysis of the literature on both the inhibition and the stimulation of the central nervous system of animals. Figure 2.A also shows that most of the studies investigated the effects of ultrasound at frequencies below 1 MHz due to the fact that, in the majority of them, US was delivered transcranially. The skull has a much higher absorption coefficient than soft tissue, which increases the amount of energy lost during the propagation of the acoustic beam. The higher the loss of energy, the higher the increase of temperature of the treated area which explains why transcranial neuromodulation must be operated at low sonication frequencies. In addition, the skull has almost an order of magnitude higher acoustic impedance, compared to the underlying brain tissue which causes impedance mismatch and scattering of the acoustic waves.

The lower the frequency, the lower the spatial resolution, resulting in a larger focus point which could influence the neural activity of areas adjacent to the one targeted by the treatment, causing their undesired stimulation or inhibition. It is therefore clear that in order to achieve high spatial resolution and target deep-seated brain regions, higher frequency must be used and its effects on the activity of the nervous system investigated. In addition, smaller focus points create a higher intensity gradient which was hypothesised to be more efficient in stimulating the neuronal activity [23].

In order to limit overheating of the tissue, pulsed wave protocols are typically preferred for ultrasound neuromodulation, for which the duration of the tone-bursts needs to be defined. The analysis of literature seems to indicate a decreasing trend in the relation between tone-burst duration and pulse repetition frequency, suggesting that shorter tone-bursts are necessary for higher repetition frequencies (Figure 2.B). In addition, it was hypothesised that neurons that have just been stimulated are more responsive to successive treatments [15].

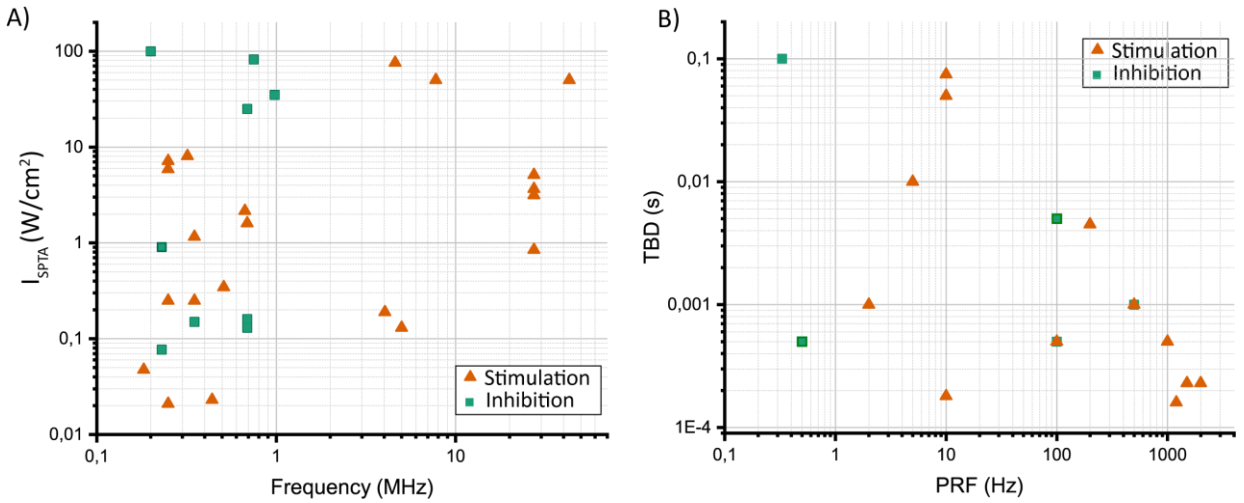

Figure 2 Sonication parameters extracted from literature. A) Relation between spatial-peak temporal-average intensity and sonication frequency. B) Relation between tone-burst duration (TBD) and pulse-repetition frequency (PRF). Orange triangles stands for studies in which stimulation was achieved while green squares for inhibition studies.

2.4 Experiment characteristics

In addition to the sonication parameters, also the type of ultrasound transducer, measurement method, experimental setup and the type of cells or animal needs to be chosen. In the studies on ultrasound neuromodulation, small size animals, such as rats, mice and rabbits, were typically used because they are easier to handle compared to the large ones. Moreover, for both *in vitro* and *in vivo* experiments, the brain areas often chosen were the hippocampus, thalamus and the different types of cortices.

In *in vivo* experiments, animals must be anesthetised to avoid bites or other injuries to the experimenters or the instruments, but the level of anaesthesia was found to heavily influence the success rate of the experiment [7], [24], [25], making it difficult to compare the results obtained by different groups. In addition, both focused and unfocused transducers were used, and especially the use of both an unfocused transducer and a small size animal poses the problem of the possible creation of constructive and destructive interference inside the brain due to the reflection of the sound waves inside the skull, which causes a discrepancy between the output pressure of the transducer and the real pressure inside the brain. A detail of the ultrasound parameters used in the analysed studies can be found in the Appendices chapter.

2.5 Goal of the project

From the previous paragraphs it is clear that, although the results are highly variable, ultrasound can excite and inhibit the neural activity in a reversible and safe way. In most of the cases, ultrasound for the modulation of the nervous system was delivered transcranially, at frequencies below 1 MHz. Although on

one side this guarantees the treatment to be non-invasive, on the other side, for areas deep inside the brain submillimetre precision cannot be achieved. In addition, piezoelectric transducers were typically used to generate the ultrasound beam, but they are bulky devices that needs to be driven by a power amplifier and a function generator, and they also contain lead, which makes them not biocompatible.

These two limitations can however be overcome by using a new technology for the generation of the ultrasound waves. Specifically, capacitive micromachined ultrasound transducers (CMUT) devices could be used instead of piezoelectric transducers. CMUTs are tiny devices, in the order of hundreds of micrometres, and can be made biocompatible. Therefore, they could potentially be implanted underneath the skull, making it possible to increase the sonication frequency, and by removing the limitation of the energy absorption by the skull, the spatial specificity of the treatment will increase. This idea is depicted in Figure 3, where CMUT devices are placed on top of the brain, therefore not requiring implantation of electrodes. By precisely steering the ultrasonic beam, deep and tiny structures can be targeted. However, investigations on the effects of high frequency ultrasound on the activity of the central nervous system have not been conducted yet.

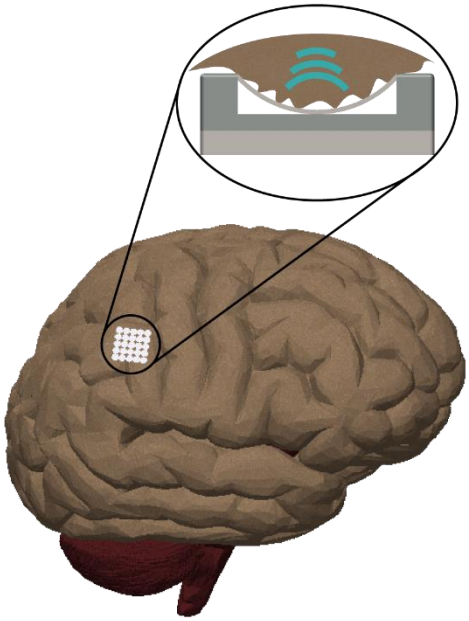

Figure 3 Schematic of ultrasound neuromodulation operated by CMUTs devices coupled to the brain.

The goal of this project is therefore to investigate the effects of ultrasound frequencies above 1 MHz on the excitability of the central nervous system. This thesis presents the design of an experimental protocol, including both the setup and various sonication protocols to be tested on *in vitro* cell preparations of mice hippocampi, comprising also cells transfected with epileptic genes. Two ultrasound frequencies are investigated, namely 5 MHz and 13 MHz, using both continuous wave as well as pulsed wave sequences combined with different treatment durations and pulse repetition frequencies.

The remainder of the thesis is organised as follows. Chapter 3 describes the materials and methods for the experiments and the analysis of the results. The results of the experiment are presented in Chapter 4, followed by their discussion in Chapter 5. Finally, Chapter 6 concludes the thesis with a summary of the achievements and Chapter 7 contains some recommendations.

3 Materials and methods

3.1 Experimental procedures

3.1.1 Cell culture

The experiments were conducted at the Erasmus Medical Center (Erasmus MC) in Rotterdam, the Netherlands. The neuronal cultures were prepared crossing FvB/NHsD females with FvB/NHsD males (both ordered at 8-10 weeks old from Envigo). Primary hippocampal cultures were used for the experiments and prepared by isolating the hippocampi from the brains of E16.5 embryos. After dissociation, the neurons were plated on coated MEA (Multielectrode Array) plates at a density of $3.5x10^4$ per well in a volume of 500 μL (detailed description of the culture preparation can be found in the methods section of [26]). The plates were stored at 37°/5 % CO_2 until the day of transfection. Half of the culture was transfected in order to induce epileptic behaviour. They will be referred to as epileptic cells in this thesis, while the non-transfected cells will be referred to as normal cells. The neurons were incubated until the culture was 28 days old. All animal experiments were approved by the Erasmus MC institutional Animal Care and Ethical Committee, in accordance with European and Institutional Animal Care and Use Committee guidelines.

3.1.2 MEA and acquisition system

The MEA plates used in this work have 24 wells, each with 12 gold electrodes coated with PEDOT (poly3,4-ethylene-dioxythiophene) plus 4 reference electrodes. Each electrode has a diameter of 30 μm and is arranged on a 4x4 grid at a pitch of 300 μm (MultiChannelSystem, Germany), illustrated in Figure 4.A-B. The extracellular signals were recorded using a commercially available acquisition system (MultiChannelSystem, Germany) at a sampling frequency of 10 kHz. In addition, the recorded data was filtered by the recording system using a 4^{th}-order low-pass Butterworth filter with a cutoff frequency of 3.5 kHz and a 2^{nd}-order high-pass Butterworth filter with cutoff frequency of 100 Hz. The activity of the neurons was recorded for five minutes before the start of the ultrasound exposure; this will be referred to as the baseline in this thesis.

3.1.3 Experimental setup

A custom lid was designed and fabricated in order to cover the MEA headstage (MultiChannelSystem, Germany) to ensure a constant ambient over the MEA plate of 5% CO_2 and 95% O_2 using an external oxygenation system interfaced to the lid *via* a small tube. The custom lid was provided with circular holes corresponding to each MEA well, to allow the US transducer to enter the well. Only two wells were used simultaneously for each of the transducer, therefore during each experiment the other holes were kept closed with a cap. A support structure for the US transducers was designed to ensure a constant height and alignment with respect to the underlying well. Alignment holes were engraved onto the lid to allow the transducer support structure to be positioned precisely with respect to the lid and the MEA well. A clamping system was also designed and fabricated to keep the MEA headstage and the lid in a fixed position with respect to each other. Figure 4.D to F depicts a cross-section of the transducers placement inside the wells and a schematic of the complete experimental setup. Details on the fabrication of the lid and of the clamping system can be found in Appendix C.

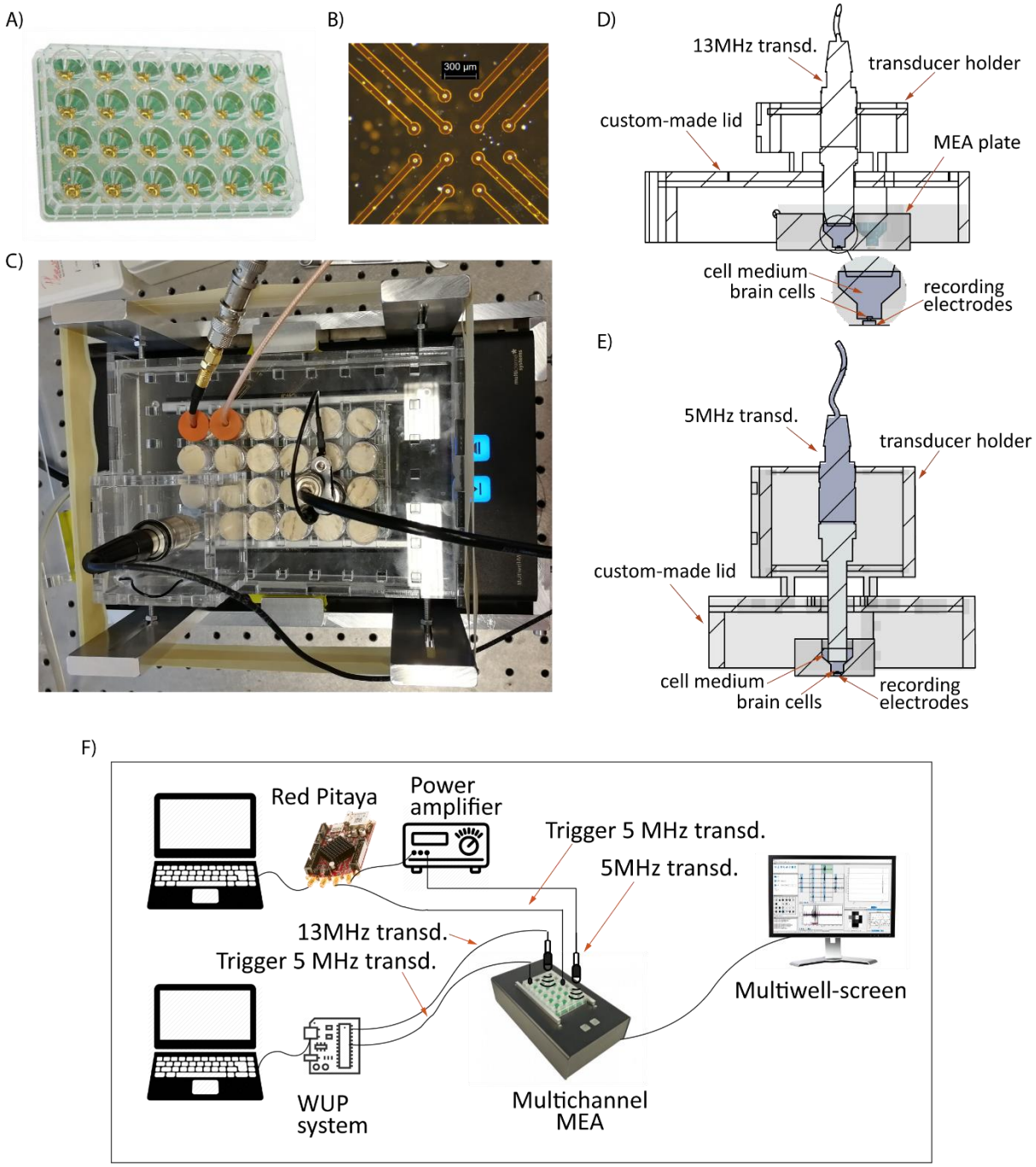

Figure 4 Experimental setup used at the Erasmus MC. A) MEA plate with 24 wells with 12 PEDOT electrodes each [82]. B) Microscope view of electrodes inside each well of the MEA, showing their arrangement. C) MEA headstage: custom transparent lid with holes aligned to every MEA well; top-left corner the two wells used for the trigger signal, and custom holder for the transducer and aluminium support to fix the lid to the MEA headstage. D) Cross-section of the experimental setup for the 13 MHz transducer, showing the relative position of the transducer with respect to the cell culture. E) Same as D) but for the 5 MHz transducer. F) Schematic of the experimental setup.

3.1.4 Focused ultrasound setup

Two focused US transducers were used in this study, namely a 5 MHz (Olympus, V310) and a 13 MHz (Olympus, V312). The former was operated with a sine wave at 5 MHz with a peak-to-peak voltage of 36 V, while the latter was driven at 13 MHz and peak-to-peak voltage of 20V, both depicted in Figure 5.C-F. The 5 MHz transducer was operated by a signal generator and a power amplifier. The signal was generated using a RedPitaya board [27]. This small credit card size board comprises two function generators that are programmable to generate arbitrary waveforms. The 13 MHz transducer was driven by a single channel of the WUP (Wireless Ultrasound Patch) system, which is a Philips proprietary, experimental 32-channel programmable ultrasound system. The Red Pitaya and the WUP system were programmed to generate an external trigger signal to indicate the start and the end of the US exposure. These signals were recorded using two of the wells (In Figure 4.D the two wells on the top left corner).

Direct measurement of the acoustic pressure at the bottom of the well is not possible in this setup. Therefore, a separate measurement was performed in a water tank setup using a calibrated needle hydrophone (Precision Acoustic Ltd) mounted on a high precision xyz scanner. The hydrophone needle was scanned in a plane perpendicular to the transducers at exactly the same distance as the bottom of the well is located from the transducers in the cell experiment (details on the pressure measurement setup can be found in Appendix A). The peak negative pressure was 0.17 MPa and 0.18 MPa respectively for the 5 MHz and the 13 MHz device (Figure 5). The corresponding mechanical indices (MI) were 0.08 for the 5 MHz and 0.05 for the 13 MHz transducer, both below the safety limit. In addition, the peak negative

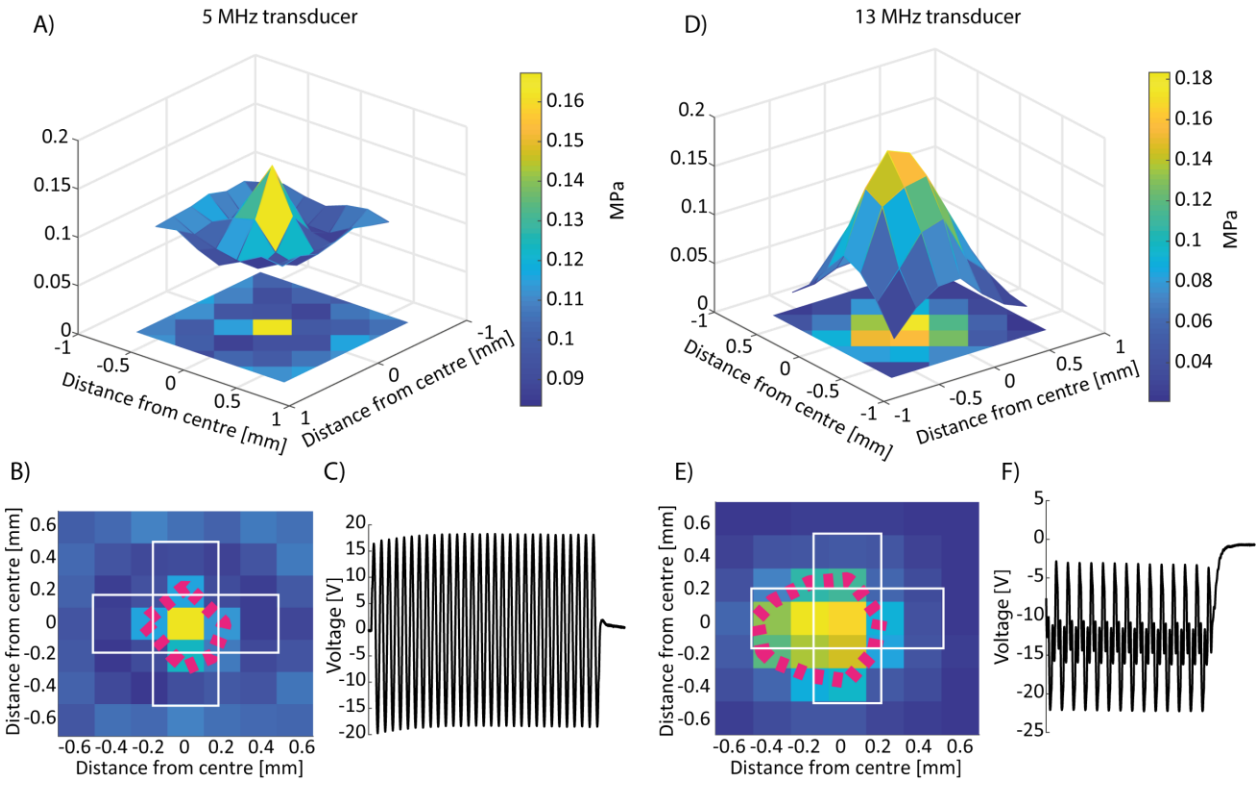

Figure 5 Pressure profiles and focus shape of the two focused transducers used during the experiment, measured with the hydrophone. A) 5 MHz transducer: shape of pressure profile. B) 2D projection of the 5 MHz pressure profile: white cross corresponds to the MEA electrodes location; magenta line corresponds to the -6 dB profile. C) Signal input to the 5 MHz transducer. D) 13 MHz transducer pressure profile. E) Projection of the pressure profile on y-z plane of the 13 MHz transducer: white cross is the area occupied by the electrodes and magenta line is the -6 dB profile. F) Signal input to the 13 MHz transducer.

pressure was below 40 MPa, which is defined as the safety limit for ensuring no cavitation-related damages [14].

3.1.5 Sonication protocol

In this section, the different sonication protocols used for the two transducers are explained. The 5 MHz transducer was driven in continuous mode for 15 and 30 seconds. The US exposure was repeated three times, with a 5 minutes observation interval between each exposure (Figure 6.A). The 13 MHz transducer was used in pulsed mode with exposure durations of 60 and 180 seconds. Also in this case, the exposure was repeated three times with an observation period of 3 minutes in between each exposure. The tone burst duration (TBD) was kept constant at 1.15 µs (15 cycles), while the pulse repetition frequency (PRF) was 800 Hz and 1 kHz for two different trials during the experiment (Figure 6.B). The different combinations of parameters tested during the experiment are summarised in Table 2, together with I_{SPPA} and I_{SPTA} corresponding to the parameters described above. Each combination was tested on a different well of the MEA. In addition, the diameter of the -6dB level of intensity was calculated to be about 400µm and 800µm for the 5MHz and the 13 MHz transducer respectively.

Table 2 Combinations neuron type-sonication parameter

Frequency	Cells type	Treatment time (s)	Observation time (min)	PRF (Hz)	I_{SPPA} (W/cm^2)	I_{SPTA} (mW/cm^2)
5 MHz	Normal	15	5	-	929.9	929.9
	Normal	30	5	-		
	Epileptic	15	5	-		
	Epileptic	30	5	-		
13 MHz	Normal	60	3	800	1.18	1.03
	Normal	180	3	1000		1.29

3.2 Data analysis

Extracellular signals were obtained using the Multiwell-Screen software application (MultiChannelSystem, Germany) which outputs the recorded signals in a proprietary data format [28]. The different files where then converted to **.hdf5* format for further processing with MATLAB®.

No additional filtering was applied to the recorded data. Recordings were inspected and electrodes with an excessively-high baseline noise level were discarded from the analysis, assuming that they were contaminated or damaged during the preparation of the cells. A spike detection algorithm based on a differential threshold was used [29]. The detected spikes were used to identify bursts of activity, defined as a sequence of closely packed spikes, separated by a time interval named inter-spike interval (ISI). The

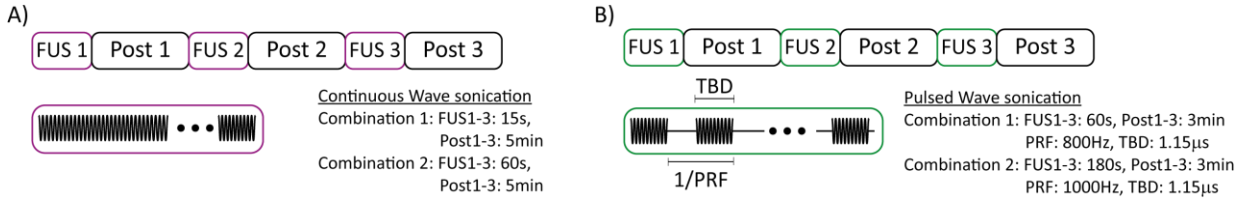

Figure 6 Diagram of the sonication protocols. A) Continuous wave sonication: three consecutive exposures to US of a different duration. B) Pulsed wave sonication: three consecutive focused ultrasound (FUS) exposures followed by an observation period and different combinations of parameters.

minimum distance between two consecutive bursts was set to 100 ms, defined as inter-burst interval (IBI) [30]. The distance between consecutive spikes inside each burst is defined as ISI in burst. These features are depicted in Figure 7.

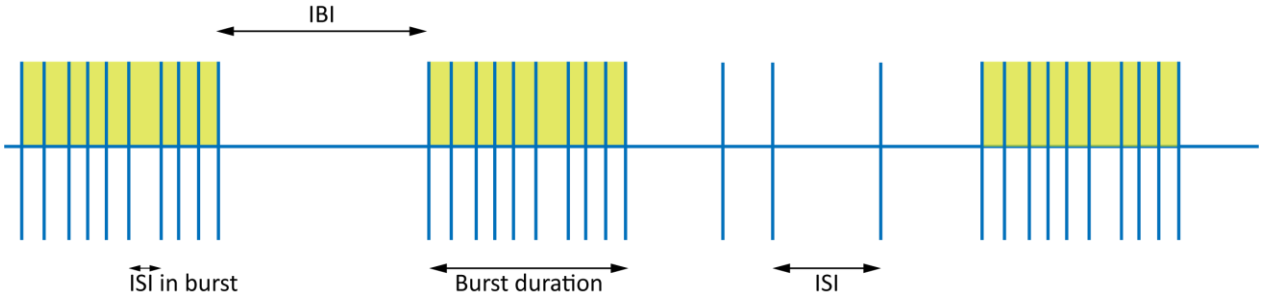

Figure 7 Spike train features. Yellow shading indicates a burst.

In addition, since multiple electrodes were recorded at the same time and the neurons inside each well behave as a collective, the spikes and bursts appear simultaneously at multiple sites. Therefore, a network burst detection algorithm was used to quantify the correlated firing among different electrodes and its variation following the US exposure of the neurons. The network burst amplitude was calculated as the product between the number of active electrodes and the number of detected spikes for each time window of 50 ms, following an approach similar to Chiappalone et al. [30]. Further details on the algorithms used for spike and burst detection can be found in Appendix B.

All numerical results were presented as median ± median absolute deviation. The significance of changes in parameters was assessed by a Friedman's test, which is the non-parametric version of the two-way ANOVA [31]. It tests the null hypothesis that there is no difference between the populations, based on the median value of the tested variable. In addition, a post-hoc Dunn & Sidak comparison [32] was carried out to test differences between the different phases of the experiment. Statistical significance was defined for $p < .05$. Statistical analysis was performed using MATLAB® built-in functions.

4 Results

In this chapter, the results obtained from the exposure of the epileptic and normal brain cells to ultrasound are presented. All figures refer to median values calculated for every valid electrode, and across all the valid electrodes of each MEA well, including also a measure of their statistical significance.

4.1 Cells behaviour

Normal and epileptic neurons showed a different firing pattern. The normal neurons were characterised by a rather irregular firing frequency, with action potentials mainly isolated from each other and few sporadic and short bursts (Figure 8.A). The epileptic cells showed a more regular firing pattern, with spikes grouped into bursts and few isolated action potentials (Figure 8.B). This characteristic behaviour was modified by the neuromodulation capability of ultrasound as described in the following paragraphs.

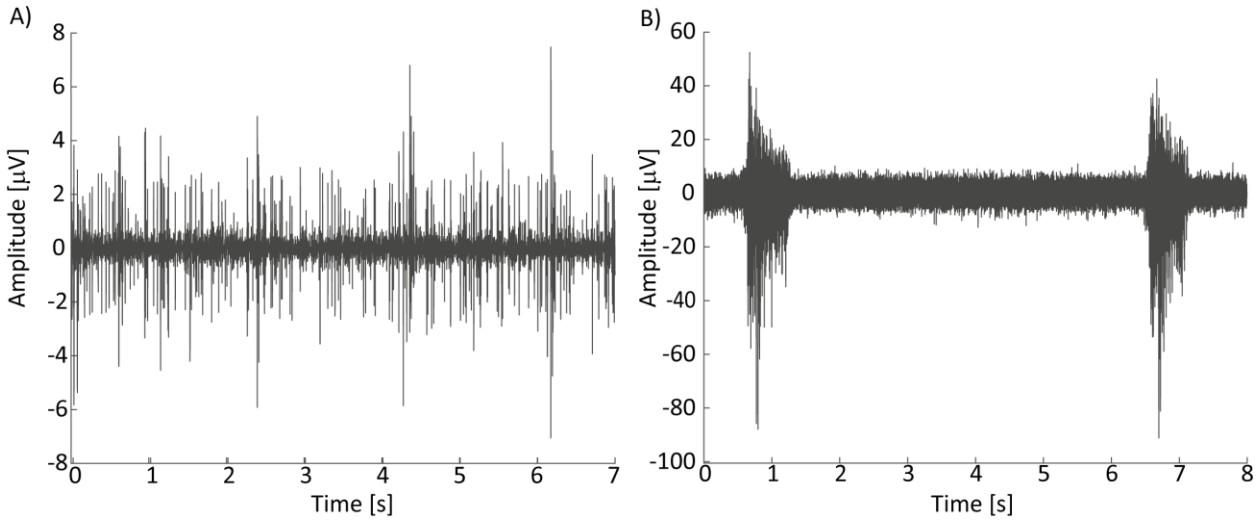

Figure 8 Spikes pattern previous exposure to ultrasound. A) Normal cells: action potentials are sparse with sporadic bursts. B) Epileptic cells: action potentials are fired in bursts and (almost) no spikes are detected in between two consecutive bursts.

4.2 Ultrasound exposure of epileptic cells

During the ultrasound exposure, the spike rate of the epileptic population increased considerably for both treatment durations compared to the baseline, as visible in Figure 9 where the green area corresponds to the period of US exposure. This was followed by a silence period after which the activity of the cells recovered to their baseline spiking behaviour, for the 15s exposure. The spike rate set to values higher than the baseline for the 60s exposure. The silence period was defined as the longest time during which no spikes were detected, represented by the light blue area in Figure 9. In addition, the spike rate of the neurons treated for one minute dropped after the first few seconds of exposure, even though the sonication continued, represented by the patterned area of Figure 9. This can also be observed in the raster plots of Figure 9 (plots in the second row of Figure 9.A-B respectively), where no spikes were

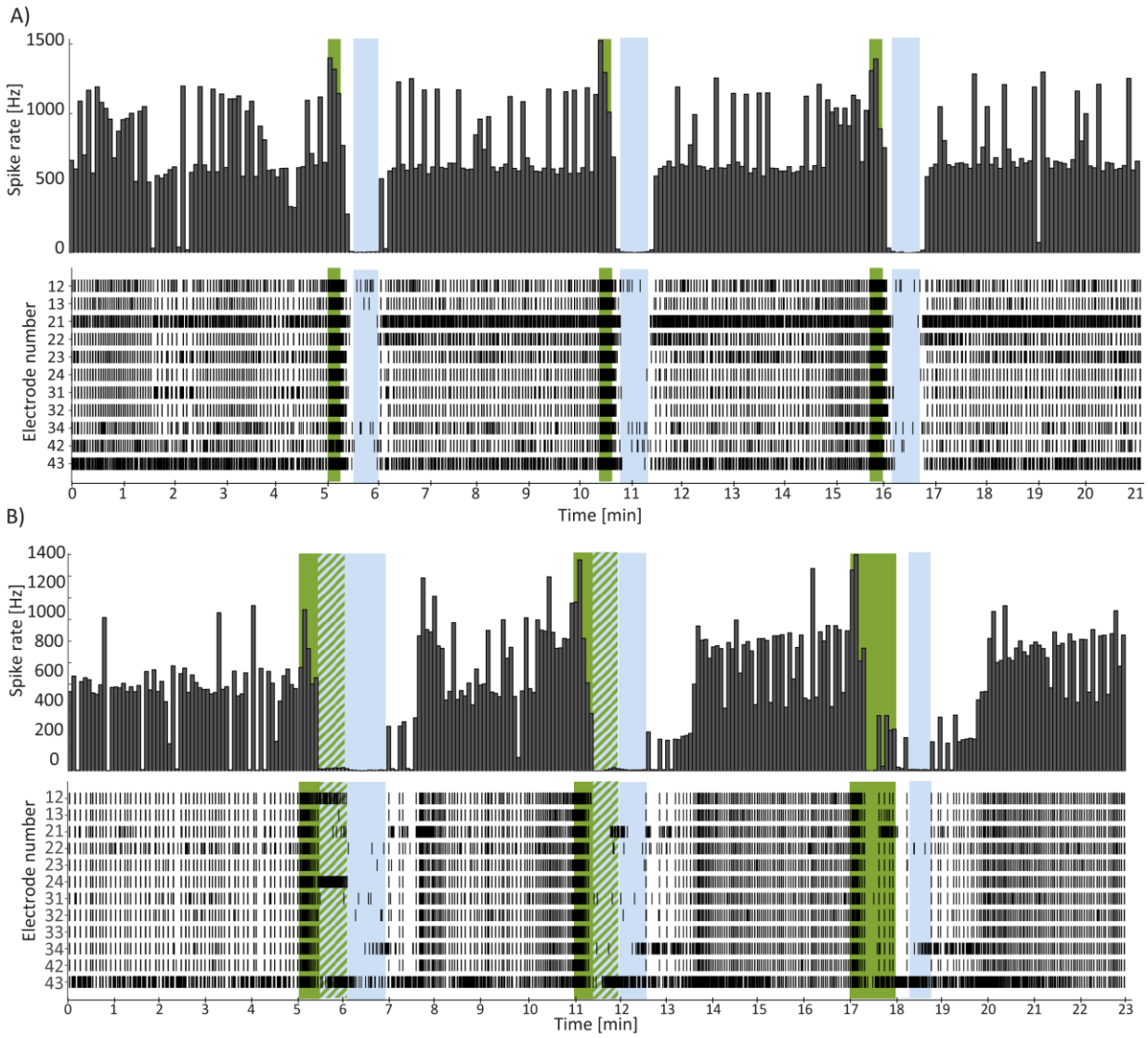

Figure 9 Spike rate and raster plots of epileptic cells for the two treatments durations. A) 15 seconds exposure: (top row) Spike rate, (bottom row) Raster plot. B) 60 seconds: same as A). Green band indicates the treatment time; light blue area indicates the silence period; patterned area indicates period of overlap between treatment and silence period. First number of the electrode number refers to electrode row; second number refers to electrode column.

detected by most of the electrodes in the area highlighted in light blue. Moreover, while the short exposure time resulted in an excitation duration and a silence period which did not show significant variation over the three consecutive exposures, the effect of the exposure for sixty seconds differed significantly between the first and the last exposure; the duration of the excitation increased while the silence period shortened (Figure 10.A-B). Ultrasound affected also the burst pattern of the spikes. Initially, the bursts had an average duration of about 350 ms, extracted from the baseline activity. This value significantly decreased during the ultrasound exposure and returned to the baseline value during the recovery period, defined as the time from the end of the silence period until the next treatment or the end of the experiment (Figure 10.C). Significant effects of the exposure to US were also seen on the time between two consecutive bursts, namely the inter-burst-interval (IBI), which was reduced by 60% for both the types of treatment (Figure 10.D), following the same pattern described for the burst duration. In addition, the sonication increased the

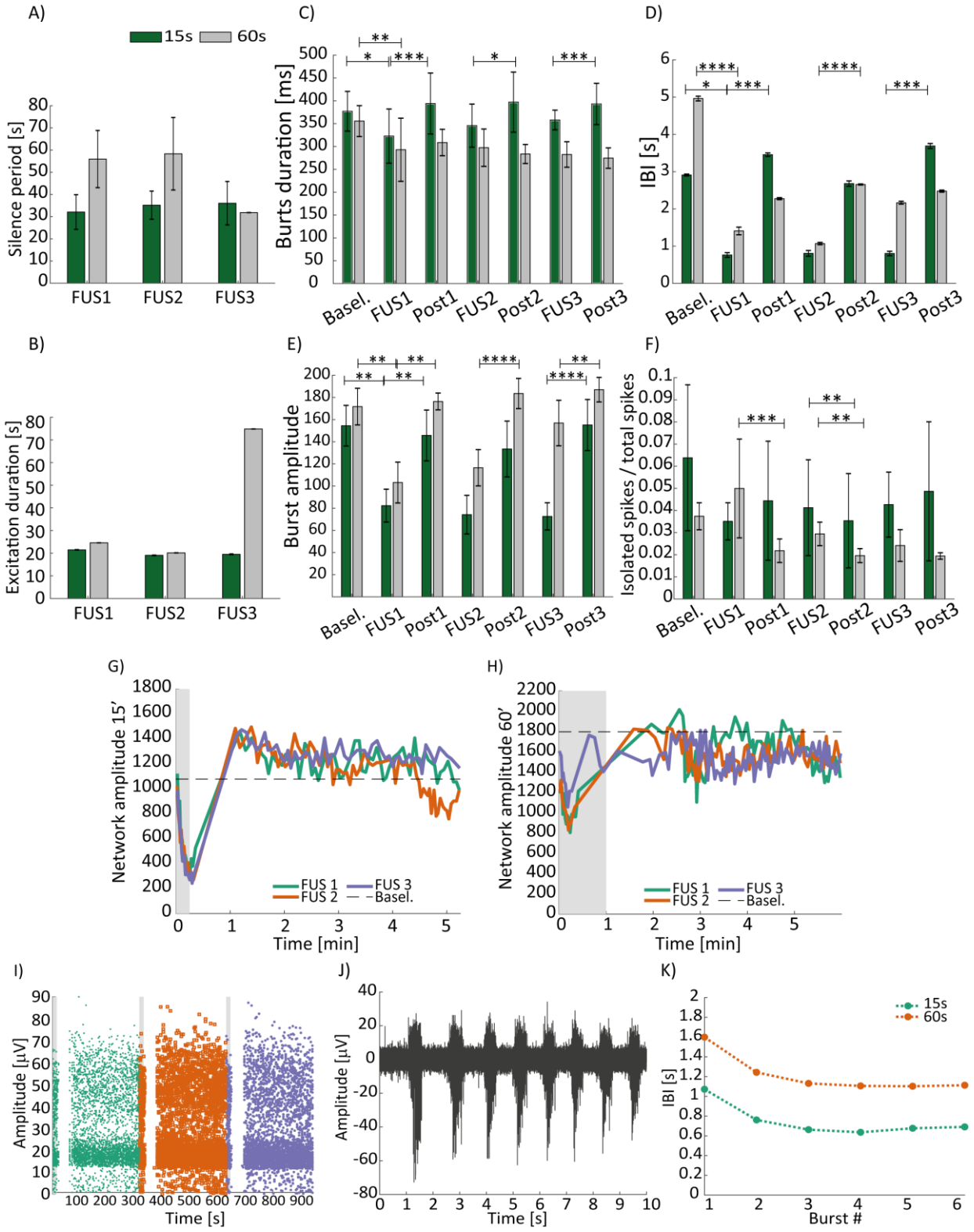

Figure 10 Effects of ultrasound exposure on epileptic cells. A) Silence period duration among the three different treatments for both the treatment durations. B) Duration of the excitation among the three different treatments. C) Burst duration comparison for the two treatment lengths. D) Inter-Burst-Interval comparison between the two treatments durations. E) Burst amplitude comparison. F) Ratio between isolated spikes and total number of spikes. G) Network amplitude trend for the 15 s treatment duration. L) Network amplitude for the 60 s treatment duration. I) Amplitude in µV of the detected spikes. J) First 10 s of the recorded signal during exposure to US. K) IBI interval of the first bursts showed in J). Different colours indicate the three sequential exposures and correspondent observation period. Plots G to I: shaded area corresponds to the treatment period. Plots C to F Friedman test: '*' p<0.05, '**' p<0.01, '***' p<0.001, '****' p<0.0001.

time between two consecutive action potentials within each burst (ISI in burst). ISI in burst can also be seen as the inverse of the spike rate in each burst, named burst amplitude as in Chiappalone et al. [30]. In fact, during the shortest exposure, the amplitude had a half-fold decrease, returning to the baseline value in the recovery periods, while for the longer ultrasound exposure, the effect of the third treatment was more moderate than for the first one, however statistically significant (Figure 10.E). Moreover, exposure for one minute to ultrasound significantly modified the spike pattern of the neurons, increasing the percentage of isolated spikes during the exposure, calculated as the ratio between the number of spikes not part of a burst to the total number of spikes, in a time window of fifteen seconds, and averaged over the corresponding phases of the experiment (Figure 10.F). The shortest exposure did not cause a meaningful variation of this percentage.

The network activity, which measures the synchrony of spikes and bursts across the recording electrodes in each MEA well, was also quantified showing two different patterns for the two exposure durations (Figure 10.G-H). During the shortest exposure, the network amplitude steeply decreased during the first twenty seconds, to later jump to values above the average of the baseline at the end of the silence period, and eventually converge to the average baseline value. Similarly, during the one-minute exposure, the network amplitude dropped during the first few seconds of the ultrasound exposure, to increase and eventually converge to the average baseline value as well. The reduction of the network amplitude was mainly influenced by the smaller number of spikes in each time window and the number of active electrodes did not decrease during the ultrasound exposure.

The spike amplitude also changed during the exposure to ultrasound. In Figure 10.I the amplitude of the spikes recorded from a representative electrode shows a reduction in amplitude during the exposure time, and a sudden sharp increase after the end of the silence period. This was followed by a decrease of the amplitude towards values recorded before the exposure to ultrasound. The decrease in amplitude during the exposure to ultrasound is visible also in Figure 10.J which depicts a detail of the signal recorded during the first ten seconds of the exposure. In addition, this figure shows that ultrasound did not have an immediate effect on the spike train and the distance between consecutive bursts started to shorten significantly only after about two seconds from the start of the exposure. Figure 10.K shows in fact the shortening of the IBI from the first to the consecutive bursts.

4.2.1 Statistical significance of cell behaviour modification due to ultrasound exposure

The results obtained from the analysis of the spike trains showed that the calculated variables do not follow a normal distribution, therefore non-parametric tests were used to assess the statistical significance of the changes in the firing patterns caused by ultrasound. Table 3 summarises the results of the statistical analysis together with the significant results of the comparison between the different phases of the experiment. There were no significant differences between the non-listed pairs.

Table 3 Summary of Friedman's test results for epileptic cells exposure to ultrasound at 5MHz

	15 seconds				60 seconds			
Variable	**χ^2**	**Df**	**p-val.**	**Signif. post-hoc comparison**	**χ^2**	**Df**	**p-val.**	**Signif. post-hoc comparison**
Burst duration	50.5	6	p < .0001	Basel.-FUS1 p < .05 FUS1-Post1 p < .001 FUS2-Post2 p < .05 FUS3-Post3 p < .001	43.3	6	p < .0001	Basel.-FUS1 p < .01
IBI	54.1	6	p < .0001	Basel.-FUS1 p < .05 FUS1-Post1 p = .0001 FUS3-Post3 p = .0001	71.3	6	p < .0001	Basel.-FUS1 p < .0001 FUS2-Post2 p < .0001
Burst amplitude	58.8	6	p < .0001	Basel.-FUS1 p < .01 FUS1-Post1 p < .01 FUS3-Post3 p < .0001	65.4	6	p < .0001	Basel.-FUS1 p < .001 FUS1-Post1 p < .01 FUS2-Post2 p < .0001 FUS3-Post3 p < .01

4.3 Ultrasound exposure of normal cells

Similarly to the epileptic cells, also the firing pattern of the normal neurons was strongly modified during the exposure to US.

4.3.1 Continuous wave at 5 MHz

The spike rate increased during both exposure durations, except for the first of the three 15s exposures. During the shortest treatment, the activity of the cells stopped for few seconds after the end of the exposure, followed by a silence period, after which the activity of the cells restarted (Figure 11.A). The spiking activity during the one-minute exposure experiment only stopped during the first of the three exposures, while during the following two, detected spikes were sporadic and the activity only reduced after the end of the treatment. This is depicted in Figure 11.B in the plots in the top row in which the spike rate does not drop to zero. This is also shown in the corresponding raster plots in the bottom row of Figure 11.B, which show that spikes were recorded during the entire duration of the experiment without any silence period for most of the electrodes. In addition, it can be noted that the spike rate of the neurons exposed for one minute, after the end of the treatment, returned to higher values than the average firing rate of the baseline (data before the first exposure in Figure 11). The duration of the excitation remained almost constant during the short US exposure while the length of the silence period was halved (Figure 12.A-B). Exposure of the neurons for one minute had the effect of doubling the duration of the excitation, while a silence period could be identified only for the first exposure since the activity did not stop after the following exposures (Figure 12.A-B).

Moreover, ultrasound was able to change the spike pattern of the normal neurons, increasing the number of isolated spikes during the exposure periods. The ISI was therefore analysed, showing a significant and permanent decrease from the start of the exposure, for both the durations (Figure 12.C). In addition, in Figure 12.C the ISI value for the baseline recording shows both a large mean absolute deviation and length since it inherently includes the distance between consecutive bursts. Bursts almost disappeared in the following phases of the experiment as a demonstrated by the decrease of both mean absolute deviation and length of inter-spike interval. In addition, since the spike pattern of the normal cells was characterised by mostly isolated spikes, with few bursts, the analysis of the bursts features was not performed.

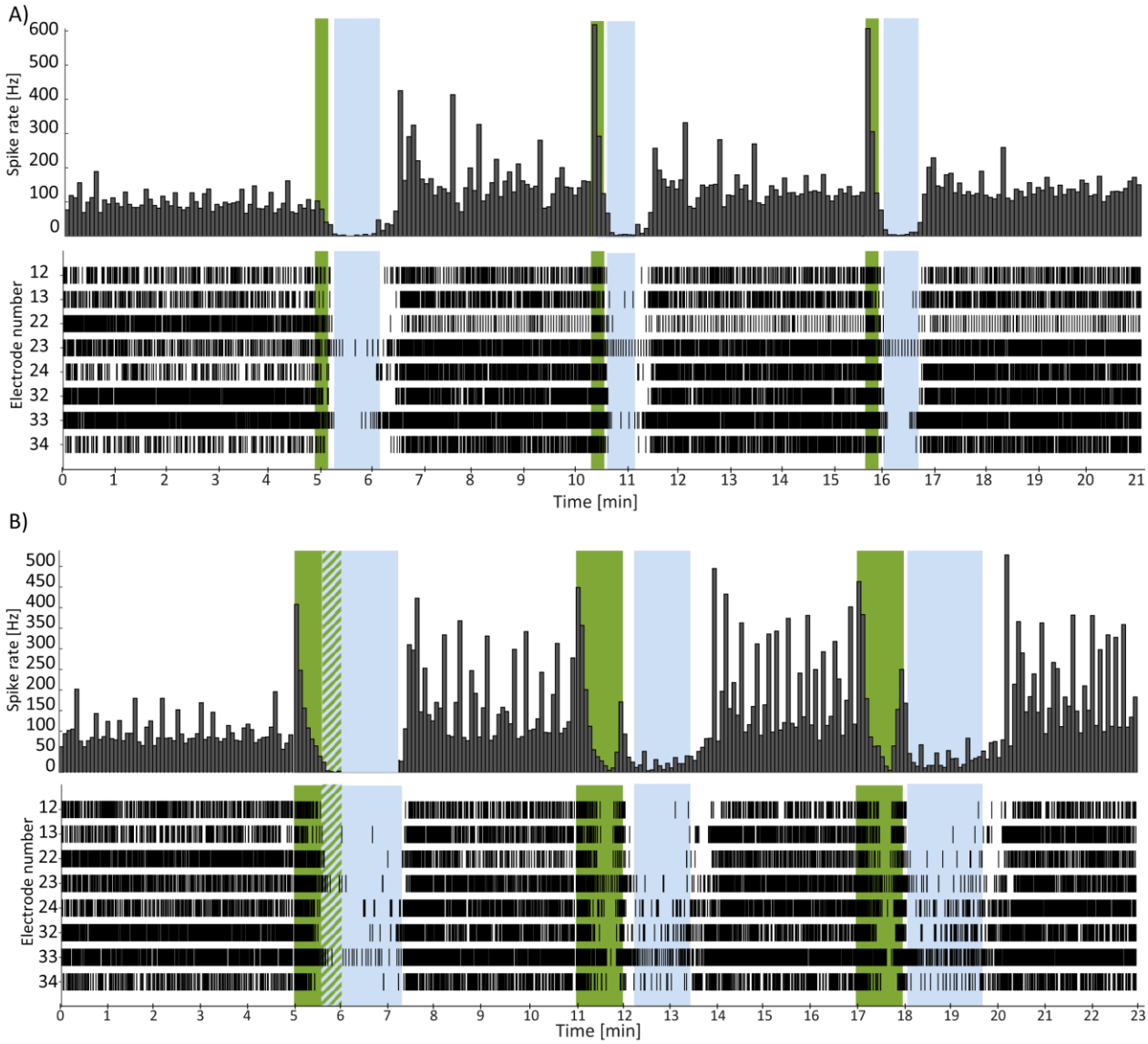

Figure 11 Spike count and raster of normal cells exposed to ultrasound at 5MHz. A) 15 seconds treatment: (top row) spike rate, (bottom row) raster plot. B) 60 seconds treatment: top and bottom row as in A). Green bar indicates the time of the treatment; light blue area indicates outlines the silence period; patterned area indicates the period of time in which cells are silent despite they are being exposed to US. Data before the first exposure refer to the baseline recording. Electrode number is coded as: first figure electrode row, second figure electrode column.

The analysis of the network amplitude highlighted an increase during the US exposure with respect to the baseline value, visible in Figure 12.D-E. The amplitude then converged to the average baseline value after the exposure to US for the short exposure duration, while for the longer sonication it did not decrease after the exposure to ultrasound. As for the epileptic cells, the increase in network activity was mainly due to the higher number of spikes in each time window.

Moreover, the amplitude of the detected spikes decreased during the exposure time to suddenly jump to higher values when the activity of the neurons recovered. The amplitude then decreased again until the next treatment or the end of the experiment (Figure 12.F). This is depicted also in Figure 12.G where the first eight seconds of exposure to ultrasound of one of the recordings are shown. This figure shows both

the decrease in amplitude of the spikes and the delayed effect of ultrasound on the excitability of the neurons, as seen for the epileptic ones.

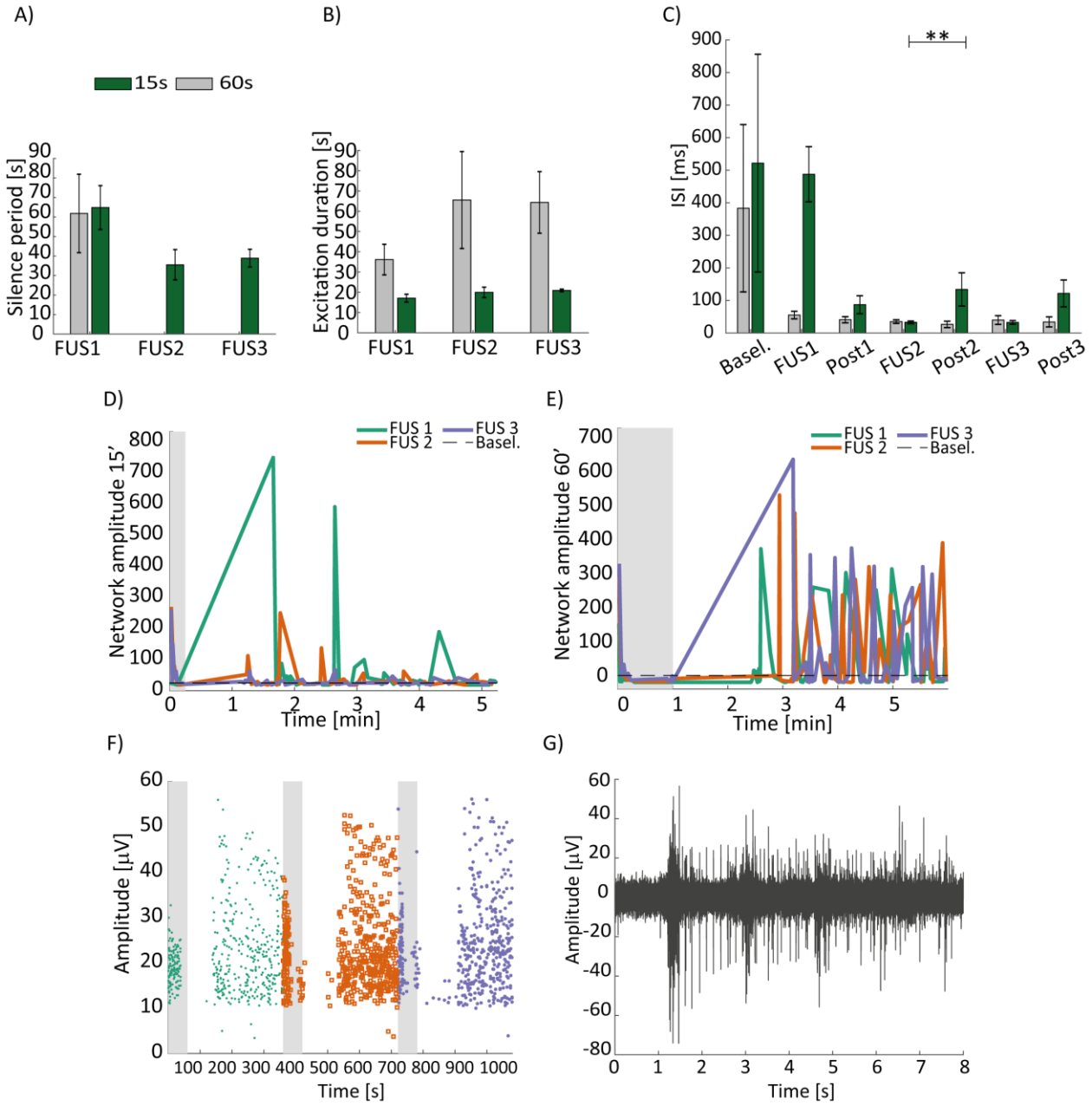

Figure 12 Effects of ultrasound exposure at 5 MHz on normal cells. A) Length of the silence period among the three different treatments. B) Duration of the excitation among the three different exposures. C) Inter-Spike-Interval comparison. D) Network amplitude trend for the 15 s exposure duration. E) Network amplitude for the 60 s exposure duration. F) Amplitude of the detected spikes for a representative electrode. G) First 8 s of recording during the exposure to ultrasound. Plot C Friedman test: '*' p<0.05, '**' p<0.01, '***' p<0.001, '****' p<0.0001. Plots D to F: grey bar indicates US exposure period.

4.3.1.1 Statistical significance of 5MHz ultrasound effects on normal cells

The variables used to describe the spike train did not show a normal distribution, therefore a non-parametric test was used to determine the statistical significance of the changes caused by the exposure

to ultrasound. The same conditions detailed in paragraph 4.2.1 hold, hence Friedman's test was used. Table 4 summarises the results of the statistical analysis, together with the ones of the post-hoc Dunn & Sidak comparisons between the different phases of the experiment. No statistical significance resulted for the pairs not detailed in Table 4.

Table 4 Summary of Friedman's test result for normal cells exposed to 5 MHz ultrasound

	15 seconds				60 seconds			
Variable	**χ^2**	**Df**	**p-val.**	**Signif. post-hoc comparison**	**χ^2**	**Df**	**p-val.**	**Signif. post-hoc comparison**
ISI	34.8	6	p < .0001	FUS2-Post2 p < .05	-			

4.3.2 Pulsed wave at 13 MHz

Neurons exposed to ultrasound at 13 MHz showed an opposite response compared to the ones previously described. In particular, their spike rate decreased during the exposure to ultrasound for both the exposure durations and it did not return to the baseline value after the end of the exposure (Figure 13). In addition, the neurons did not silence during or after the end of the exposure. As a consequence, variations in the firing pattern were mainly observed between the baseline and the first ultrasound exposure. The inter-spike interval increased for both the exposure durations and set to values higher than the baseline condition (Figure 14.A). In addition, Figure 14.A shows a high median absolute deviation, depicting the presence of both isolated spikes and bursts in the spike train.

The network amplitude did not vary significantly among the different phases of the one-minute exposure experiment, oscillating between values below the average of the baseline (Figure 14.B). Exposure for three minutes, on the other hand, caused a decrease of the network amplitude, especially during the first treatment, and the amplitude did not converge to the average of the baseline (Figure 14.C). In addition, the analysis of the amplitude of the detected spikes did not show any significant change during the exposure to ultrasound.

4.3.2.1 Statistical significance of normal cells reaction to 13MHz ultrasound

Spike train metrics did not follow a normal distribution also in this case. Results of Friedman's test are summarised in Table 5 together with the significant results of the comparison between conditions. No-statistically significant results are not displayed in Table 5.

Table 5 Summary of Friedman's test for exposure to ultrasound at 13MHz

	60 seconds				180 seconds			
Variable	**X^2**	**Df**	**p-val.**	**Signif. post-hoc comparison**	**X^2**	**Df**	**p-val.**	**Signif. post-hoc comparison**
ISI	-				54.9	6	p < .0001	Basel.-FUS1 p < .0001

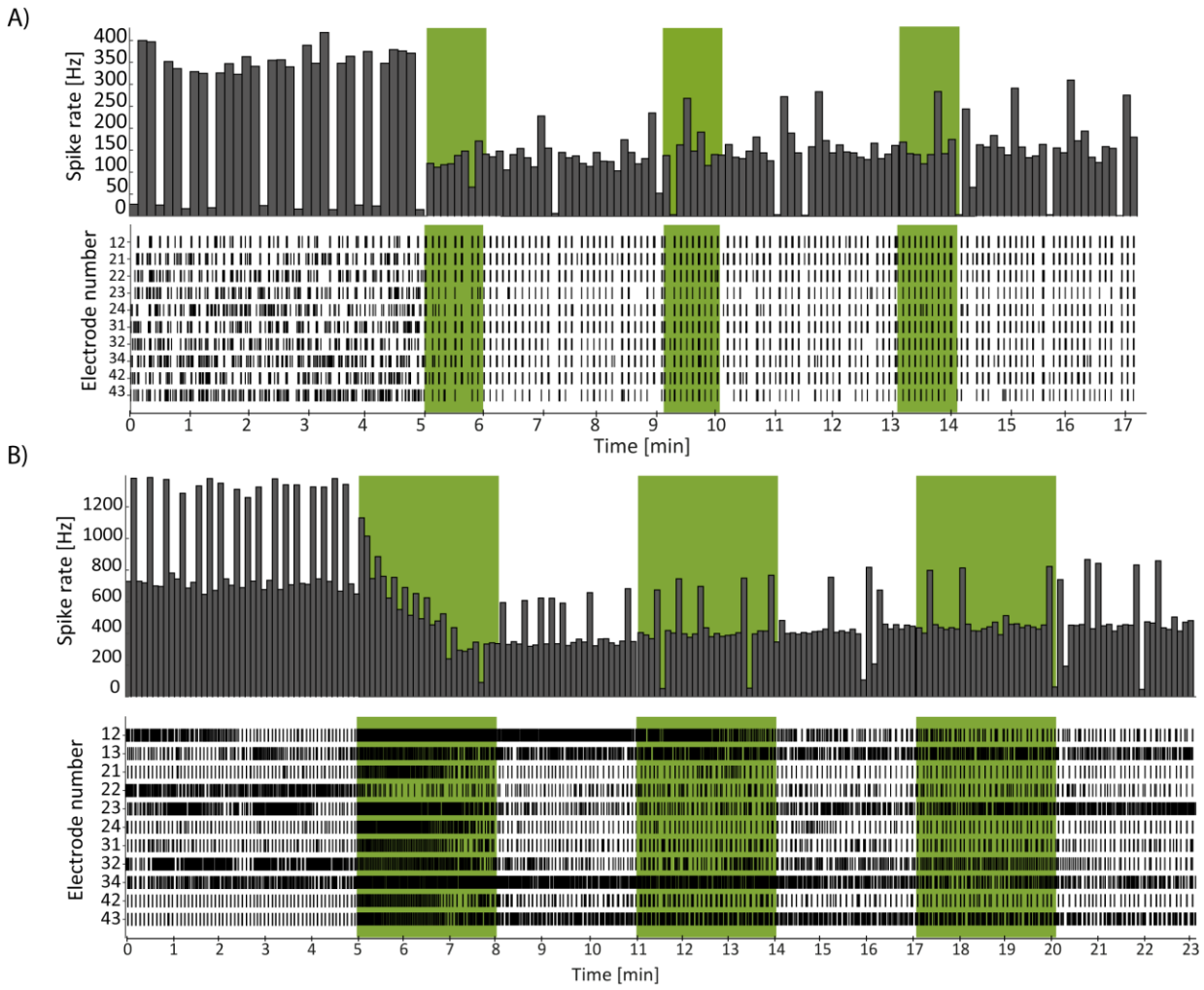

Figure 13 Spike rate and raster plots for normal cells exposed to ultrasound at 13 MHz. A) Exposure for 60 seconds. B) Exposure for 180 seconds. Green area indicates the period of exposure to ultrasound.

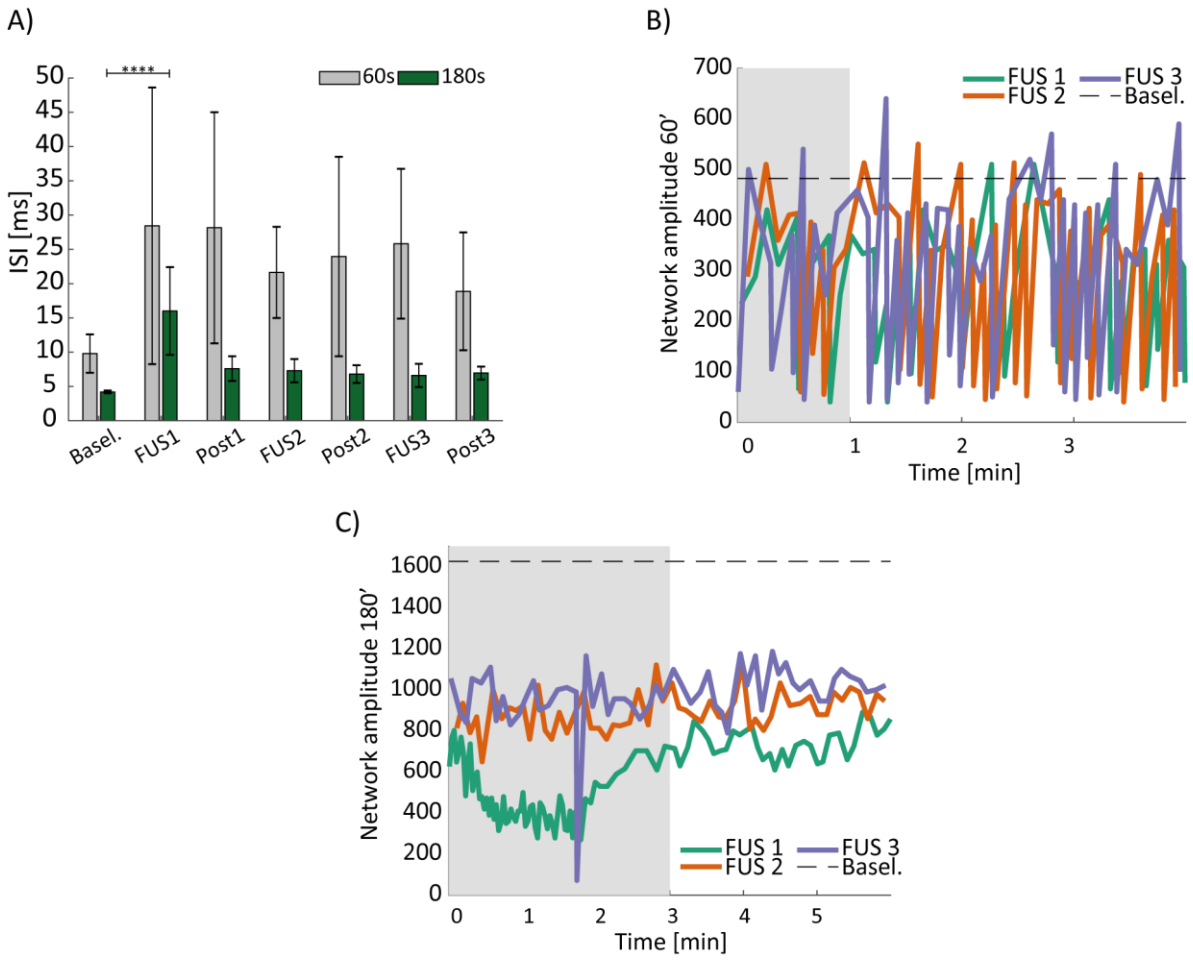

Figure 14 Reaction of normal cells to ultrasound at 13MHz. A) Inter-spike interval. B) Network amplitude for the 60s exposure duration. C) Network amplitude for the three minutes exposure. Graphs A: comparison between the two treatment durations; Friedman test: '*' p<0.05, '**' p<0.01, '***' p<0.001, '****' p<0.0001. Plots B-C grey area corresponds to ultrasound exposure time.

4.4 Focusing effect of ultrasound

The 5 MHz device, due to the strong reaction it caused in the sonicated cells, made it possible to observe the focusing effect of ultrasound. The effect of the sonication at the different electrode locations in the MEA wells was analysed, considering the residual activity during the silence period following each of the three treatments. It was observed that only peripheral electrodes were still active during this period. In Figure 15 a heatmap of the electrode activity is drawn based on the total number of detected spikes in a time frame of three seconds during the silence period. It refers to the activity of a representative well, however the same phenomenon was observed for all the other wells sonicated with the 5 MHz transducer.

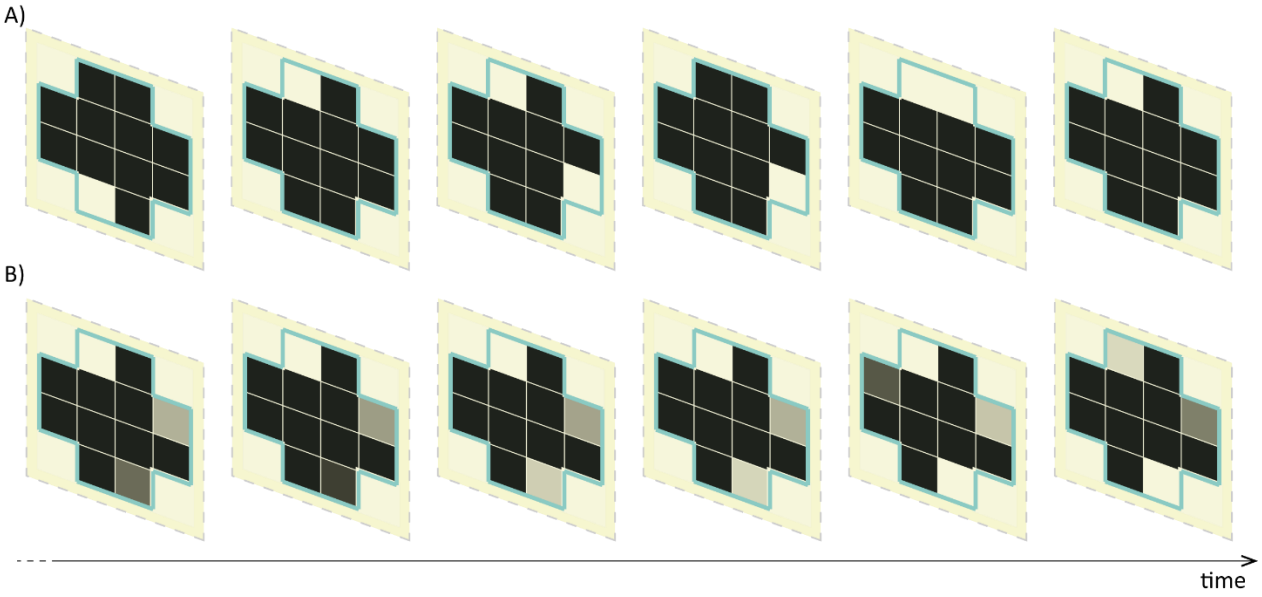

Figure 15 Focusing effect of the 5 MHz transducer. A) Residual activity during the first silence period after the first 15 s exposure. B) Residual activity during the first silence period after the first 60 s exposure. Colour code: black corresponds to zero activity and white corresponds to maximum activity. Each frame represents the activity calculated on a time windows of 3 s.

4.5 Ultrasound effects on spikes shape

The shape of the spikes recorded from the electrodes located in the centre of the focus point was analysed to assess if ultrasound exposure caused any change on them. The shape of the spikes was extracted starting from 1 ms previous the position of the peak up to 3 ms after. The shapes were then aligned based on the position of their peak and for each electrode they were analysed before, during and after exposure to ultrasound. For both normal and epileptic cells, the detected spikes were categorised in two groups: spikes with positive polarity and spikes with negative polarity (Figure 16 and Figure 17). Hence, it was assumed that the spiking activity of at least two neurons was recorded by each analysed electrode. However, when exposed to ultrasound, epileptic and normal cells showed a different reaction.

In the epileptic culture, during the period of acoustic sonication, both neurons with spikes of positive and negative polarity were excited, as shown in Figure 16.B-C-D. On the other hand, exposure to ultrasound of neurons of the normal cell culture, silenced one of the two groups of neurons. After the exposure, both positive and negative polarity neurons started firing again (Figure 17.B-C-D).

To quantify the effects of ultrasound on the shape of the action potentials, spikes of negative polarity were chosen and extracted for each phase of the treatment. Their average shape was then calculated and compared among the different phases of the experiment for both types of neurons (Figure 16.E-F-G and Figure 17.E-F-G). Although the calculation of the full-width at half-maximum (FWHM) did not show any significant difference between the different spikes shapes, Figure 16.E-F-G and Figure 17.E-F-G show a clear modification of the average spike profile, especially for the normal neurons. The negative slope of the spikes, corresponding to the depolarisation phase, started about 0.1 ms earlier and the repolarisation phase was shifted forward of about 0.3 ms, compared to before and after the ultrasound exposure. In addition, ultrasound increased the duration of the refractory period. After the exposure to ultrasound, the average shape of the spikes converged to the shape recorded before the sonication. Epileptic neurons

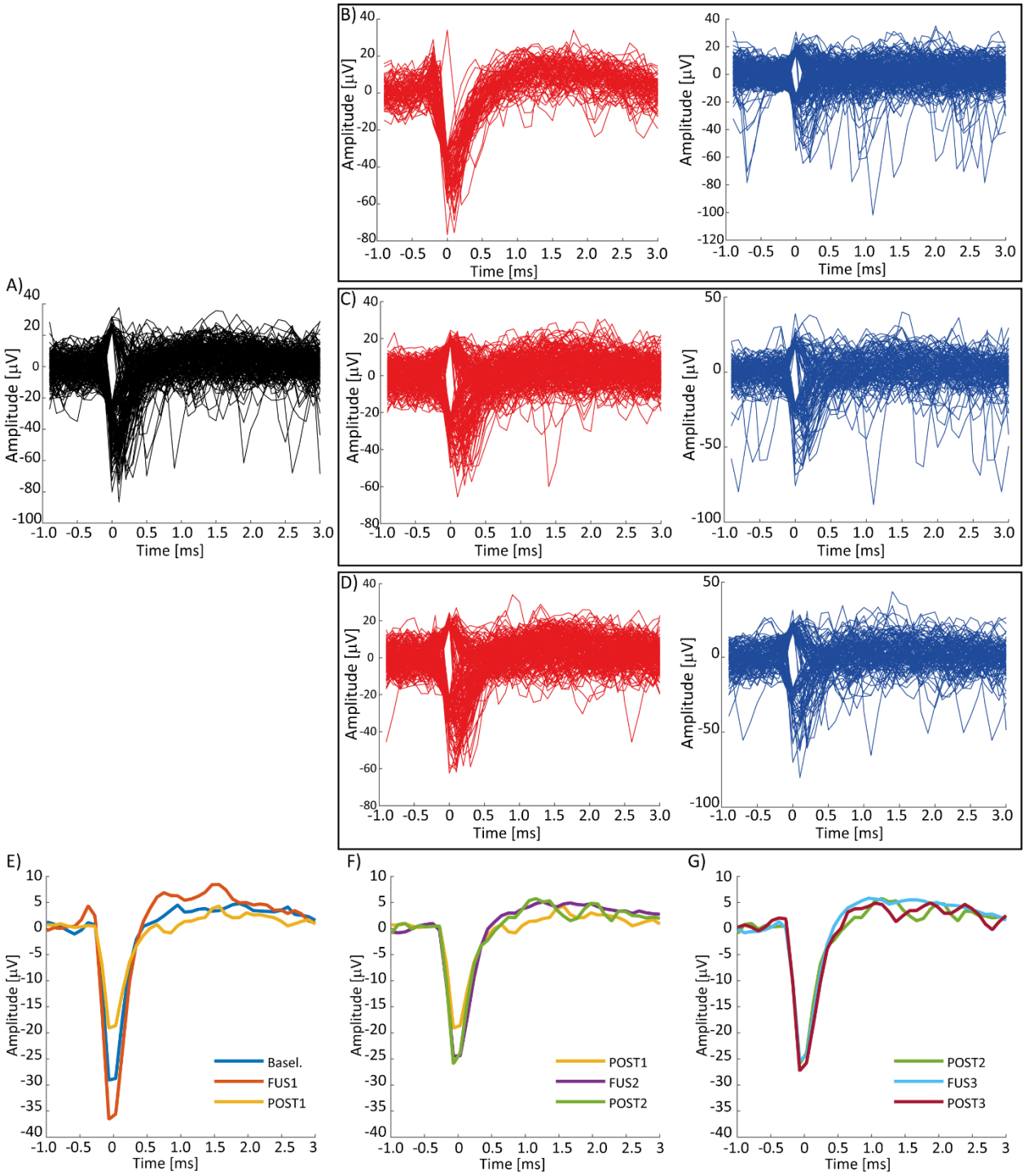

Figure 16 Effects of ultrasound at 5 MHz on the shape of the spikes of epileptic cells. A) Spikes waveforms during baseline. B) Red waveforms are the spikes recorded during the first exposure to ultrasound; blue waveforms refer to the recovery period. C) Same as B) but for the second exposure and after-exposure. D) Same as A) but for the third exposure and after-exposure. E-F-G) Comparison among the average spike waveforms previous, during and after exposure to ultrasound.

showed a comparable behaviour, although the shape was significantly modified only during the first of the three exposures. During the following ones, the average shape was similar to the one of the baseline.

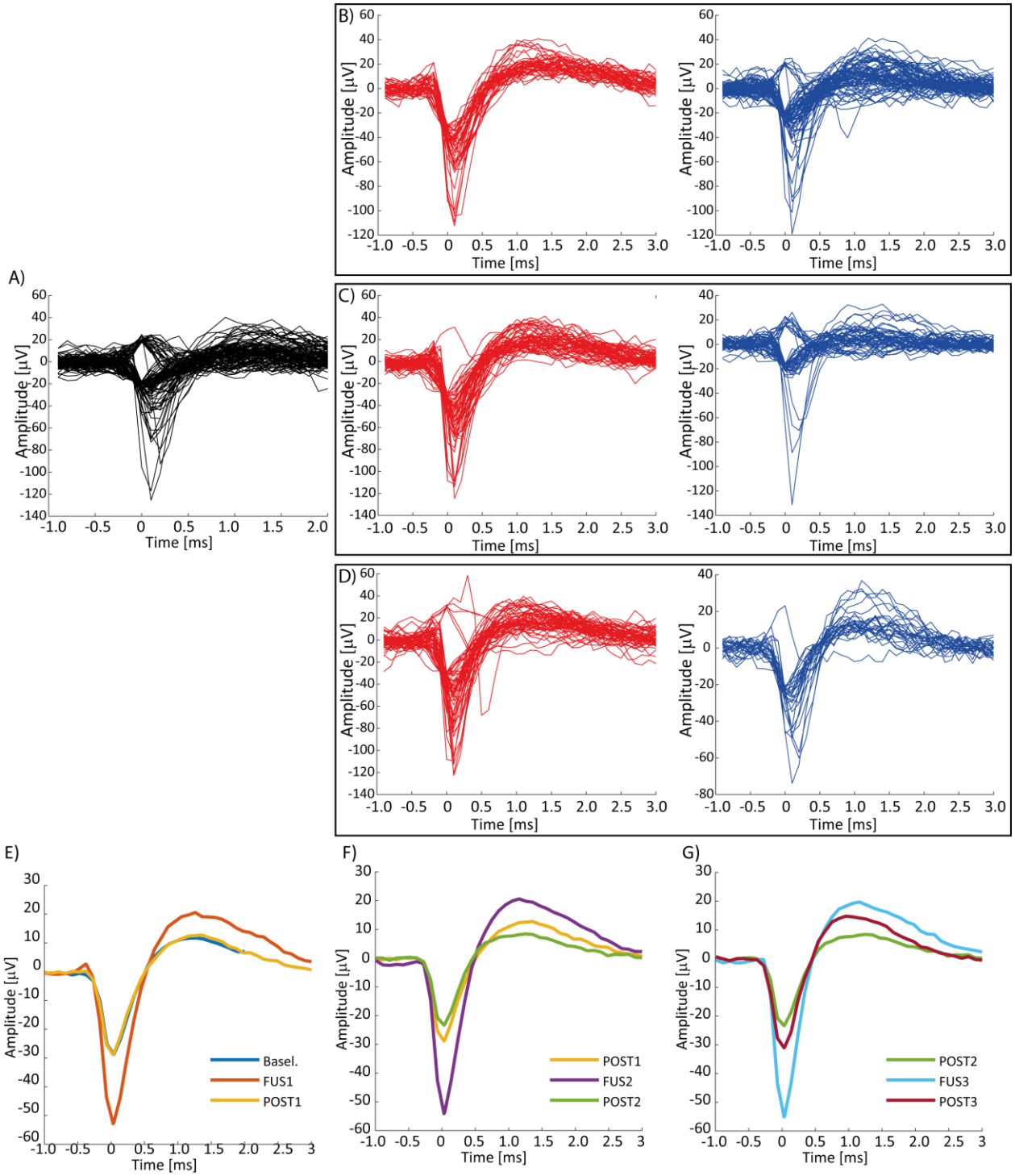

Figure 17 Effects of ultrasound at 5 MHz on the shape of the spikes of normal cells. A) Spikes waveforms during baseline. B) Red waveforms are the spikes recorded during the first exposure to ultrasound; blue waveforms refer to the recovery period. C) Same as B) but for the second exposure and after-exposure. D) Same as A) but for the third exposure and after-exposure. E-F-G) Comparison among the average spike waveforms previous, during and after exposure to ultrasound.

4.6 Estimation of intensity and thermal index for brain sonication

The results described above confirmed the set of parameters used in this experiment were able to modulate the activity of the sonicated neurons. Therefore, in this paragraph, an estimation of the intensity and thermal index in case of using the same protocol for direct sonication of the brain is given. The average absorption coefficient and specific heat capacity of brain tissue were used for this calculation (values obtained from [33]). The thermal index for soft tissue (TIS) was computed, as described in Bigelow et al. [34]:

$$TIS = \frac{W_0 \cdot f}{210 \frac{\mathrm{mW}}{\mathrm{MHz}}} \tag{4.1}$$

Where W_0 is the maximum value of time averaged acoustic output power and f is the sonication frequency, in MHz. Table 6 summarises the values of the estimated parameters inside the brain for the two sonication frequencies.

Table 6 Estimate of the sonication parameters inside the brain

	5 MHz	**13 MHz**	
PRF	-	800 Hz	1000 Hz
I_{SPPA} (W/cm^2)	1.77	2.12	2.12
I_{SPTA} (mW/cm^2)	883.70	1.95	2.44
TIS	0.026	< .01	< .01

5 Discussion

In this study, the neuromodulation capabilities of ultrasound at high frequencies were demonstrated. Two sonication frequencies, 5MHz and 13MHz, and different combinations of parameters were tested on both normal and epileptic cell cultures, showing a stronger reaction for the latter. Focused transducers were used for the experiments, which modified the firing pattern of epileptic and normal cells.

5.1 Effects of 5MHz continuous wave focused ultrasound on epileptic and normal neurons

Normal and epileptic cells cultures were exposed to focused ultrasound at 5MHz using a continuous wave protocol and both similarities and differences emerged from the analysis of the results. For both types of neurons, two exposure durations were tested and both resulted in excitation of the cells. The excitation was followed by a silence period or a period of minimal activity. The reason for this silence period after the end of the sonication can be explained by an over-excitation of the neurons. During excitation, neurons increase the release of neurotransmitters which creates a momentarily toxic environment, resulting in the cessation of the activity for a brief period. In addition, when ultrasound was delivered for more than twenty seconds, the firing rate of the neurons decreased (Figure 9 and Figure 11) which could also be explained from the fact that the neurons are not able to maintain the high level of activity for more than a certain period. This could be advantageous in case of epileptic cells where the spike rate could be lowered by simply exhausting them with ultrasound exposure.

For the epileptic neurons ultrasound shortened both the interval between bursts and the duration of the bursts. Also the spike rate inside each burst dropped during the exposure to ultrasound. Shorter burst duration and lower spike rate are related to the smaller number of spikes in each burst whose reason could be found in the biophysical mechanisms responsible for ultrasound neuromodulation, which will be discussed later.

Two different patterns were observed for the network amplitude, which could find an explanation in the different way ultrasound affected the inter-spike interval of the two types of culture. The decrease of burst amplitude and the lower number of spikes in each burst, for the epileptic neurons, explains the decrease in network amplitude observed for this type of cells during the sonication period (Figure 10.G-H). On the other hand, the lower ISI in the normal culture during the period of exposure to ultrasound can explain the increase in network amplitude during this phase.

The spike pattern of epileptic cells is mainly composed of bursts with a few isolated spikes, as demonstrated by the extremely low ratio between isolated spikes and total spikes (Figure 10.F). Ultrasound was able to modify this pattern, increasing the number of spikes outside the bursts, in particular for the longer exposure. On the other hand, the activity of the normal culture was mainly composed of isolated spikes, and exposure to ultrasound did not further increase their ratio to the total number of detected spikes.

5.2 Influence of intensity, continuous wave and pulsed wave sonication on normal cells

The effects of both continuous and pulsed wave sonication were tested on normal cells, however at two different ultrasound frequencies and three orders of magnitude different I_{SPTA}.

Continuous wave sonication excited the neurons, causing an increase of their firing rate during the period of exposure, while ultrasound delivered in pulsed wave inhibited the neurons, decreasing their firing rate. The significant difference in I_{SPTA} and the different sonication frequency might be responsible for the opposite neuromodulation effects observed during the experiment, therefore a correct comparison of the effects of the two types of sonication protocols is not possible in this case and the response of the cells should be evaluated either for the same intensity, or for the same sonication frequency.

In addition, two different pulse repetition frequencies were used for the pulsed wave sonication: 800Hz and 1000Hz. The inter-spike interval increased for both of them and the network activity set to values below the average baseline amplitude.

Although it is not possible to determine which is the key sonication parameter that caused the different reaction of the cells to CW and PW ultrasound, it might be inferred that, since the neurons were inhibited for both the pulse repetition frequencies, this parameter was not determinant in the stimulation or inhibition of the neural activity of the cells. In addition, for the best of the author's knowledge, no studies were conducted on the inhibition of the neurons at frequencies above 1 MHz, and no trend could be highlighted based on those values. However, for the same sonication frequency, typically higher intensities were used for inhibition compared to stimulation (Figure 2.A). It is therefore not clear why, in this experiment, inhibition was achieved at lower intensities compared to stimulation and it might be that, at different sonication frequencies, the importance of the biophysical mechanisms responsible for the response of the cells to the ultrasound is also different. In addition, another contributing factor might be the fitting of the transducer inside the MEA well. The 13 MHz device, in fact, had almost the same diameter as the well, therefore leaving only a small gap around it for the CO_2/O_2 mixture to reach the culture. This might have increased the inhibition of the cells. It is therefore not possible to draw a conclusion based on these results and more experiments need to be performed to determine which is the key parameter that discriminates between stimulation and inhibition of the neurons.

5.3 Influence of the duration of the exposure to ultrasound

Continuous and pulsed wave sonication were delivered with two different exposure durations, which caused the sonicated neurons to behave differently. Normal and epileptic neurons were exposed to continuous wave ultrasound for 15 and 60 seconds at 5 MHz. For both cells types, the changes in the spike train pattern caused by the shortest treatment duration were reversible, and the features of the firing pattern returned to values comparable to the ones of the baseline. On the other hand, exposure to ultrasound for one minute had a different effect among the three consecutive treatments and the firing pattern features did not tend to return to the baseline value after the exposure. Also the spike rate remained higher than before the exposure to ultrasound, meaning that a longer exposure to ultrasound affected the excitability of the neurons for a longer period. It can therefore be assumed that this period is longer than five minutes, since the activity of the sonicated cells was recorded for five minutes after each treatment and during that time the spike rate of the neurons remained higher than the baseline. The duration of the excitation increased from the first to the last of the exposures, shortening the silence period. In addition, normal cells did not silence after the first of the long exposures, which might suggest

that neurons that are just being sonicated are more excitable and have a stronger response to the following sonications.

5.4 Focusing effect, biophysical mechanisms and general considerations

In this work, two focused transducers were used, whose focusing effect was demonstrated analysing the level of activity recorded by the electrodes during the silence period and showing residual activity only at peripheral electrodes locations. However, no significant differences in activity level emerged in the period of exposure to ultrasound. It might therefore be that, although the -6dB level of the transducer was smaller than the area covered by the recording electrodes, the intensity outside this contour was higher enough to activate also neurons lying outside it.

In addition, a preliminary analysis of the effects of ultrasound on the shape of the recorded spikes showed that exposure to ultrasound significantly affected the profile of the spikes. The reason for this effect can be found on the possible biophysical mechanisms responsible for the neuromodulatory effects of ultrasound. Mechanical effects on the mechanosensitive channels and the acoustic cavitation are likely to be accountable for the reaction of the cells to US. In fact, the change of the spikes shape observed during the period of exposure, suggests that ultrasound had an effect on the activation of Na^+ channels. The earlier start of the depolarisation phase can be explained by an increased number of Na^+ channels driven by the ultrasound waves. Consequently, the ionic flow of sodium from outside to inside of the cells increases driven by its concentration gradient [35]. This can also be considered responsible for the higher amplitude of the average spikes shape recorded during the exposure to ultrasound. In addition, the possible creation of pores due to the expansion and contraction of nanobubbles inside the lipid bilayer of the membrane can also be accountable for the modification of the shape, further increasing the flow of Na^+ and K^+ across the membrane of the neurons. In addition, the mechanism by which pores are created is an indirect mechanism which can explain the delayed reaction of the cells to ultrasound highlighted for both normal and epileptic cells (Figure 10.J-K and Figure 12.G). Moreover, the increased length and amplitude of the refractory period can explain the increased inter-spike interval inside each burst observed in the epileptic culture. Due to the longer refractory period, the time between consecutive spikes needs to be longer to allow the cell membrane potential to return to the resting state. This effect was not visible for the normal cells because their inter-spike interval was two orders of magnitude longer than the duration of the refractory period, therefore not highlighting this phenomenon.

The opposite polarity of the spikes recorded by the electrodes is due to the relative position of the neurons with respect to the recording electrode. However, during exposure to ultrasound of the normal culture, one of the two types of neurons was silenced. Therefore, it could be hypothesised that ultrasound stimulated inhibitory neurons which then caused an inhibitory synapse on the neighbouring cells. This effect was however clearly visible only during the first of the exposures of the epileptic neurons.

Spatial-peak pulse-average intensities used in this work were below the safety limits. I_{SPTA} values for the continuous wave sonication were about 200 mW/cm^2 higher than the limits imposed for ultrasound imaging, however other groups have used intensities much higher than the one used in this work, and they have reported no damage to the sonicated tissue. In addition, since the safety limits refer to ultrasound imaging, it has already been argued that they might be too conservative for ultrasound neuromodulation. Moreover, the culture exposed to intensities higher than the safety threshold either recovered to the behaviour previous the treatment or kept a higher fire rate, meaning that no apparent damage was caused by the exposure and confirming the reversible effects of ultrasound neuromodulation.

Intensity and thermal index for soft tissue (TIS) were also computed to estimate their values in case the same sonication protocol would be used for an *in vivo* experiment. Also in this case they were below the safety limits.

6 Conclusion

The effects of high frequency ultrasound on the excitability of *in vitro* cell preparation of mice hippocampi were analysed, including also cells transfected with epileptic genes. Both continuous wave and pulsed wave protocols were designed for two different sonication frequencies above 1 MHz. An existing MEA recording system setup was adapted for the use with focused piezoelectric transducers by designing a custom lid and a support system. Two opposite cell behaviours were observed depending on the ultrasound frequency. Ultrasound at 5 MHz had an excitatory effect on the neural activity of both normal and epileptic neurons, while ultrasound at 13 MHz caused the inhibition of the healthy type. For the 5 MHz protocol, I_{SPTA} was in line with the trend of values obtained from literature while for the 13 MHz, the value was much lower than what reported in literature [36]–[41]. In addition, for the best of the author's knowledge, inhibition of the neural activity at frequencies higher than 1 MHz was not investigated before.

The modification of the spike pattern features during the period of exposure to ultrasound was statistically significant in most of the cases. Ultrasound varied also the shape of the action potentials, increasing the duration of the width of the spikes and the length of the refractory period. It was also demonstrated that treatment durations in the order of one or more minutes had a stronger effect on the excitability of the cells, prolonging their excitation or inhibition for minutes after the end of the exposure.

Moreover, the focusing ability of the transducers was also analysed, showing that the effects of ultrasound on the excitability of the neurons were weaker outside the focus of the beam. This, together with the results showing the great impact on the excitability of the cells, highlights the tremendous potential of high frequency focused ultrasound for the treatment of neurological disorders. Although further investigations on the effects of a broader range of sonication parameters and their optimisation need to be done, the positive outcome of this experiment opens the way for the fabrication of high frequency CMUT devices that could be implanted under the skull and, in the future, potentially replace the current available treatments for neurological disorders.

7 Recommendations

Recommendations for the presented research include:

- Investigations on the effects of pulsed wave ultrasound at higher intensities using the same sonication protocol, to analyse if the delivery of a higher amount of energy will increase the excitability of the neurons instead of causing their inhibition. In addition, investigate the effects of pulsed wave ultrasound at 5 MHz to determine the most effective between CW and PW protocols.
- Increase the waiting time following the exposure for one minute or more to determine the duration of the excitation.
- Design new sonication protocols to determine which is the shortest exposure time still able to excite the neurons. This will also allow to test the effects of PW ultrasound on normal neurons.
- Improve the experimental setup. In particular:
    - Use MEA with denser recording electrodes, in order to better analyse the excitatory activity of the cultured cells and the focusing ability of the transducers.
    - Use MEA wells with bigger diameter such that the 13 MHz transducer could better fit into it.
    - Improve the processing of the data using specific software or optimise the code for the analysis and creation of the figures, to speed up the analysis
- Investigate the effects of ultrasound using patch clamp measurements such that the effects on a single neuron could be investigated.
- In the future, consider performing the experiment *in vivo* on a small size animal but using CMUT devices encapsulated in a suitable biocompatible material.

ULTRASOUND POWER TRANSFER FOR ACTIVE IMPLANTABLE DEVICES USING TRAPPED CHARGE CMUTs

8 Introduction

Implanted bioelectronics, also called electroceuticals or implantable biomedical device (IMD), are revolutionising the world of medicine enabling the artificial stimulation or inhibition of excitable tissue to modulate and control the immune response and the physiological functioning of organs [42]. The best known devices included in this category are pacemakers, cochlear implants, deep brain stimulators, vagus nerve stimulators and retinal implants. Thanks to the progress in technology and materials, their size is becoming smaller and smaller, reducing the need for invasive surgeries and the associated consequences [42], [43]. In addition, miniaturising the implants allows them to be placed in close proximity to the area to be treated, reducing the length of the connecting wires or even eliminating the need for them. An example is represented by the SetPoint Medical device, which consist of a miniaturised stimulator, of the size of a pill, that can be implanted directly on the vagus nerve, shown in Figure 18.A-B [44]. As a consequence, also the power supply for these devices needs to become smaller, which remains one of the biggest challenges. IMDs require on average up to few mW of power [45], and batteries are the most common method to provide this energy. However, they have a limited lifetime, they are usually of large size, and contain chemicals [46]. Alternative power sources were therefore investigated, mainly including bio-fuel cells, piezoelectricity, thermoelectricity and electrostatics. Yet, they face multiple challenges and often the amount of power these sources are able to provide is barely enough for an IMD [45].

The research for methods to wirelessly transfer power through the body has therefore increased in the past decade, highlighting three main alternatives: inductive coupling, radio frequency and ultrasound power transfer, whose schematic representation is depicted in Figure 18.C. Inductive coupling is based on the concept of the mutual inductance between two coils, an external and an implanted one. Power in the order of tens of mW can be transmitter, but several constraints exist with respect to the alignment and distance between the two coils [47]. In fact, for distances bigger than few centimetres, the magnetic field generated by the external coil rapidly loses strength before coupling with the implanted receiver [48]. In addition, the dimensions of the receiving coil need to increase proportionally with the distance from the transmitting coil, making this method not suitable for both power transfer and miniaturisation of deeply implanted devices [49].

Radio waves allowing for mid and far field transmission, also require a pair of antennas, however with no need for direct coupling. One of the major disadvantages of this method is the spreading of the waves away from the source, with only a fraction reaching the receiver and being converted into power for the IMD [49]. In addition, regulations on the safe use of microwaves limits the amount of power that is allowed to be transferred. Therefore, if on one side this method would allow power to be transferred over bigger distances compared to inductive coupling with a relatively small receiver, on the other hand the available power at the receiver side would only be in the order of microwatts to a few milliwatts [49], [50].

These two methods clearly work but when it comes to shrinking the dimensions of the implant and placing the device deep inside the body, their efficiency in transferring power decreases dramatically [49]. Ultrasound has therefore gained interest over inductive coupling and radio waves because, compared to RF, it can be focussed in the body due to its short wavelength in tissue [7].

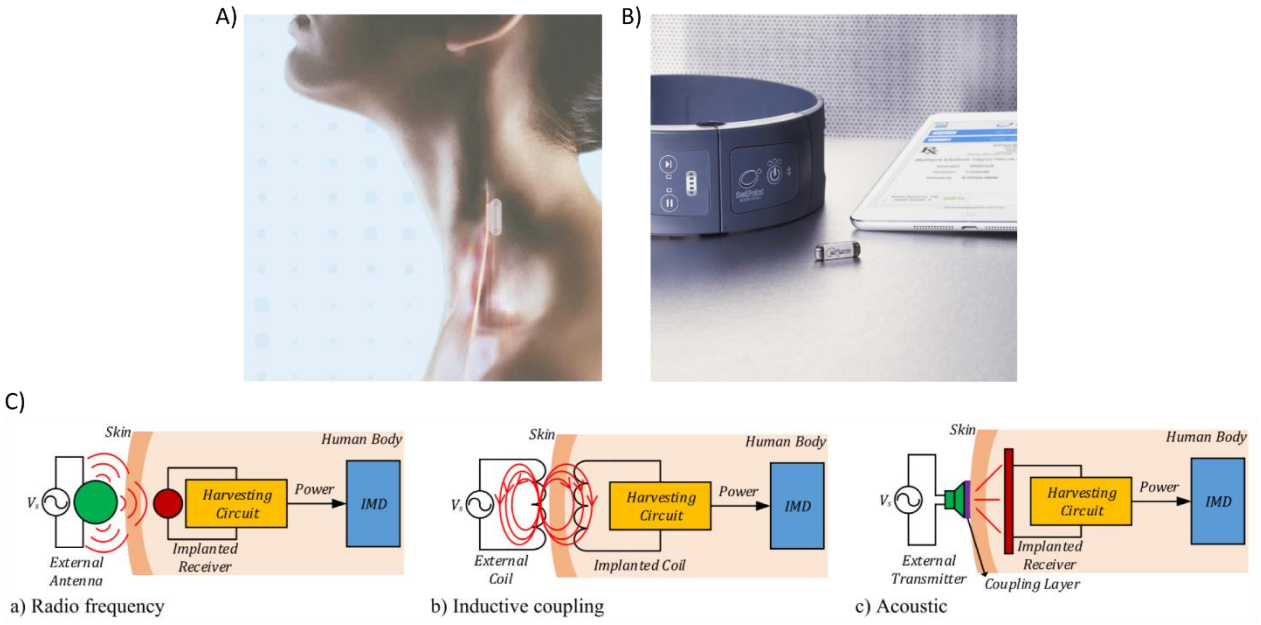

Figure 18 A) SetPoint Medical device implanted on the vagus nerve. B) SetPoint Medical Platform composed of the stimulating device, the inductive charger and the prescription pad. A) and B) reproduced from [44]. C) Wireless power transfer methods. *Figure reproduced from* [49].

As a result, relatively high power levels can be delivered at large implantation depths (> 5 cm) requiring relatively small receivers, in the order of millimetres or smaller.

Moreover, acoustic waves are safe to use in the human body at diagnostic intensities [51] and they can travel in water-based media, like the human body, with low attenuation. They are generated by ultrasound transducers which can be piezoelectric transducers or capacitive ultrasound transducers. The former makes use of the piezoelectric effect, which is an intrinsic property of a material, of which the most widely used is PZT (lead zirconate titanate), therefore they contain lead, which is not a biocompatible material and they are rather difficult to manufacture.

Alternatively, CMUTs (capacitive micromachined ultrasonic transducers), based on MEMS technology, can be used. They are composed of two conductive plates (also called electrodes), separated by a dielectric and a vacuum gap (Figure 19.A). Their dimensions are in the order of tens of micrometres, and are fabricated on silicon chips as in Figure 19.B. They offer several advantages compared to piezoelectric

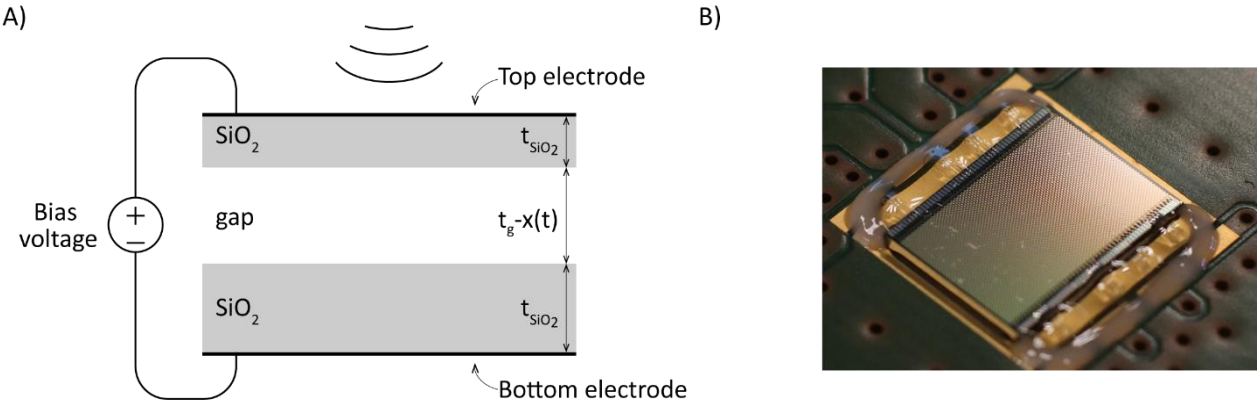

Figure 19 CMUT appearance. A) Cross-section of CMUT basic structure. B) Picture of several arrays of CMUTs mounted on a PCB; figure reproduced from [83].

transducers. They have a broader bandwidth, they are based on MEMS technology, therefore they can be batch fabricated, reducing costs, allowing array fabrication as well as scalability [52] and they can be made biocompatible, and therefore have a great potential as a wireless power source for IMDs.

They have two modes of operation: transmitting and receiving. In transmitting mode, an AC voltage is applied across the two electrodes, causing the top electrode to displace relatively to the bottom electrode. This happens because an electrostatic force is generated between the two plates, which attracts or repulses them from each other according to the applied voltage. Acoustic waves are therefore produced in the surrounding medium. In receiving mode, CMUTs can detect incoming acoustic waves. A fixed voltage is applied between the two electrodes and the incoming pressure waves displace the top membrane generating a displacement current. This mechanism is then used to evaluate the pressure acting on the CMUT [53].

CMUTs are typically operated in collapse mode for better performance and to increase their operation frequency. This is done applying a DC bias voltage across the two electrodes which is high enough to make the top membrane collapse to the bottom one. However, they do not become in direct contact because of the dielectric layer between them (Figure 19.A). In this mode of operation, the membrane assumes an inverse bell-shape, and a larger area of the membrane vibrates, compared to the uncollapsed mode.

Yet the need for an external bias voltage, which is in the order of tens of volts is not practical for a device to be implanted into the body. A possible solution has been found based on the concept of an electret microphone [54], [55]. It consists of designing the device in such a way that charges are permanently trapped in the dielectric, consequently generating an electric field between the top and the bottom electrode able to collapse the CMUT.

Charges can be trapped mainly in two different ways: in the fabrication process or by applying a DC bias voltage higher than the collapse voltage across the two electrodes, after its fabrication. The latter method is more common and in the past, other researchers have used it to prove the concept of charge-trapping in a CMUT [56]–[59]. However, in order to test the performance of their charged devices, active elements were used to amplify or filter the output signal.

8.1 Goal of the project

The goal of this project is to prove the concept whether or not it is possible to use CMUT devices with charges trapped within the dielectric to receive enough power to potentially power an implantable device, without the use of any active element. This part of the thesis therefore presents a CMUT with a modified structure, capable of permanently trapping charges in its dielectric. The characteristics of the load to be connected in order to obtain the maximum output power and a method to determine the efficiency of the ultrasound power transfer are also described.

This part of the thesis is organised as follows. Chapter 9 presents the CMUT used in this work, defines the characteristics of the load to be connected and describes the experimental setup. The results of the characterisation of the CMUT and of the power transfer are presented in Chapter 10 and discussed in Chapter 11. Chapter 12 contains a summary of the achievements and some recommendations.

9 Materials and methods

9.1 Structure of the CMUT

The CMUT devices used in this work have round shaped membrane with a diameter of 85μm and a structure composed as follows. The dielectric layer beneath the top electrode is a layer of SiO_2 with a 50 nm thickness. The dielectric layer on top of the bottom electrode consists instead of three layers, $SiO_2/Al_2O_3/SiO_2$ with a thickness of 50 nm, 200 nm and 50 nm respectively. The vacuum gap in between the two dielectrics has a thickness of 500 nm. This structure is depicted in Figure 20.

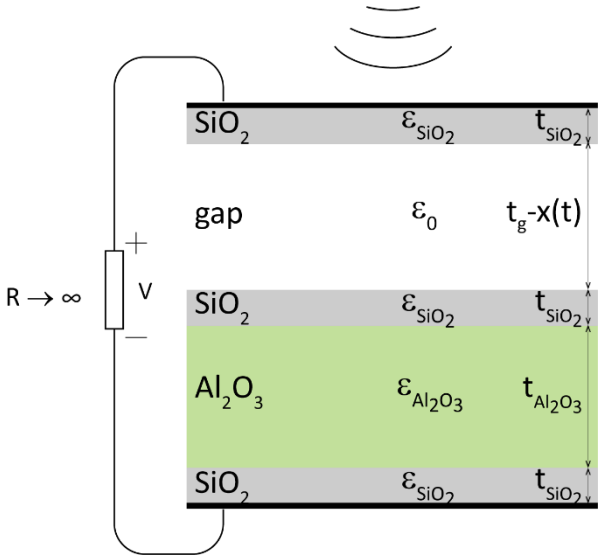

Figure 20 Composition of the CMUTs used in this work

CMUTs were arranged in arrays connected in parallel and operated in receiving mode. 56 CMUT devices were connected in one row and six of them aligned adjacent to each other and connected together; this amounts to a total of 336 CMUT devices connected in parallel which corresponds to a total occupied area of less than 2.2 mm^2. In addition, their collapse voltage was about 40V.

9.2 Charging the CMUT devices

In the devices used in this work, an Al_2O_3 layer is used as a dielectric. Al_2O_3 is a high-*k* material, known to trap a considerable amount of charges [60]. The trapped charges are considered to be permanently confined in the dielectric, being isolated by two layers of SiO_2.

The application of a DC bias voltage was chosen as a method to charge the devices, since they were already fabricated. The DC bias voltage must be high enough to create a large electric field such that the charges could travel through the dielectric and, at the same time, lower than the limit for the dielectric breakdown.

After verifying the conditions for the dielectric breakdown, A DC bias voltage of 200 V was applied for 3 hours. The value of the resulting electric field was calculated using the two fundamental relations of electrostatics:

$$\sigma = E \cdot \epsilon \quad \text{and} \quad E = \frac{V}{d} \tag{9.1}$$

Where σ is the surface charge density on each layer of dielectric, E is the electric field generated into it and ε its permittivity. The electric field is in turn dependent on the applied voltage V and on the thickness of the dielectric *d.* Assuming that the surface charge density is the same for every layer, the electric field in each layer of dielectric was calculated. The following results were obtained:

$$E_{SiO_2} = \frac{\sigma}{\epsilon_0 \cdot \epsilon_{SiO_2}} = 8.5 \cdot 10^8 \ \frac{V}{m}$$
$$E_{Al_2O_3} = \frac{\sigma}{\epsilon_0 \cdot \epsilon_{Al_2O_3}} = 3.6 \cdot 10^8 \ \frac{V}{m} \tag{9.2}$$

Where

$$\sigma = V \cdot \frac{\epsilon_0 \cdot \epsilon_{SiO_2} \cdot \epsilon_{Al_2O_3}}{3 \cdot \epsilon_{Al_2O_3} \cdot d_{SiO_2} + \epsilon_{SiO_2} \cdot d_{Al_2O_3}} \tag{9.3}$$

Both the dielectric strengths of SiO_2 and Al_2O_3 are higher than the applied electric field, therefore no dielectric breakdown was caused. Due to the charge trapping ability of Al_2O_3, after the removal of the bias voltage, the charges remained in the dielectric resulting in CMUTs with a built-in bias voltage.

9.3 CMUT model derivation

CMUTs can be modelled as a two-port network in which one port describes the mechanical domain and the other one describes the electrical domain [53]. In the mechanical domain, a mass-spring-damper (m-k-b) system can be used to model their physical behaviour, while in the electrical domain, they can be described as a variable capacitor (C_e) [53], [61], [62]. Figure 21 shows the complete model, where P represents the acoustic pressure acting on the membrane and I(t) the current circulating in the device as a result of the membrane displacement due to P. A transformer with ratio Γ connects the two ports of the model, allowing to move from one energy domain to the other.

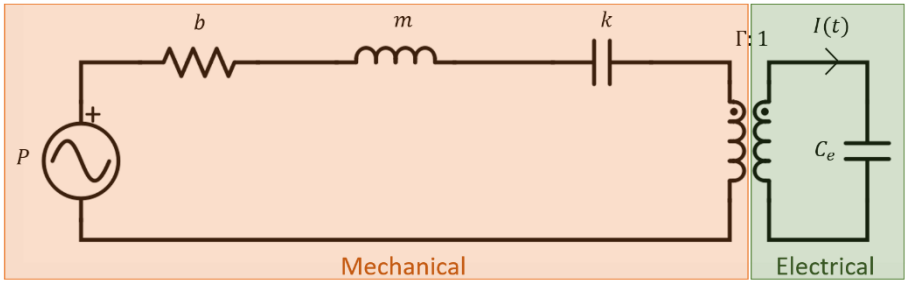

Figure 21 CMUT two-port model

The two-port model in Figure 21 can be simplified and converted in the electrical domain only. Figure 22 depicts the final electrical model in which R_m is the electrical equivalent of the damper (*b*), L_m the equivalent of the mass (*m*) and C_m of the spring (*k*). The pressure P is transformed into a voltage source V_s.

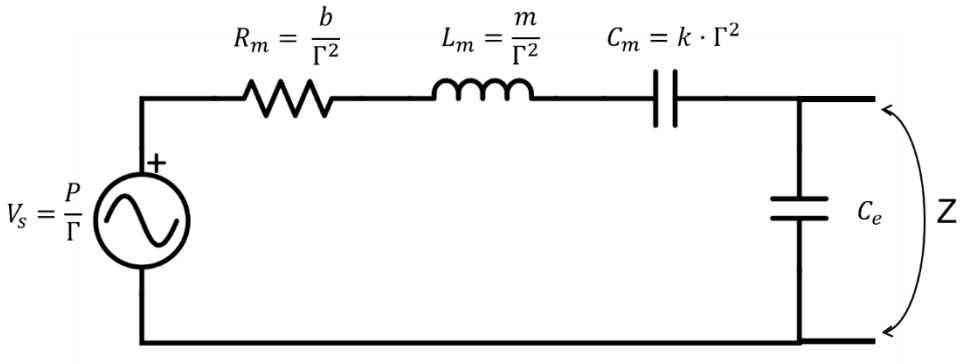

Figure 22 CMUT electrical model

9.3.1 Frequency response

In the electrical model of Figure 22, the inductor, the two capacitors and the voltage source have a frequency dependent behaviour. Therefore, to predict the device behaviour, an expression that models its equivalent electrical impedance, *Z(s)* where $s = j2\pi f$ in the frequency domain, can be written:

$$Z(s) = \frac{s^2 + \frac{R_m}{L_m}s + \frac{1}{L_m C_m}}{C_e s\left(s^2 + \frac{R_m}{L_m}s + \frac{C_m + C_e}{L_m C_m C_e}\right)}. \tag{9.4}$$

The values of the components were not known a priori. The impedance spectrum of the devices was therefore measured and eq. (9.4) fitted to it to extrapolate them.

9.4 CMUT energy harvesting

In order to harvest the maximum amount of power at the load, the maximum power transfer theorem was used, which states that the load impedance, Z_l, must be equal to the complex conjugate of the equivalent impedance of the source connected to the load, Z_s. Operating the device at its resonance frequency, L_m and C_m compensate each other. This can also be verified computing the two complex zeroes of eq. (9.4) which correspond to the resonance point of the series of R_m, L_m and C_m. At resonance, the equivalent circuit of the device is then composed of R_m and C_e only. To comply with the maximum power transfer theorem, C_e must be compensated using an inductance. In addition, a resistor needs also to be

connected. Figure 23 depicts the equivalent circuit of the CMUT in resonance with its series and load impedance highlighted.

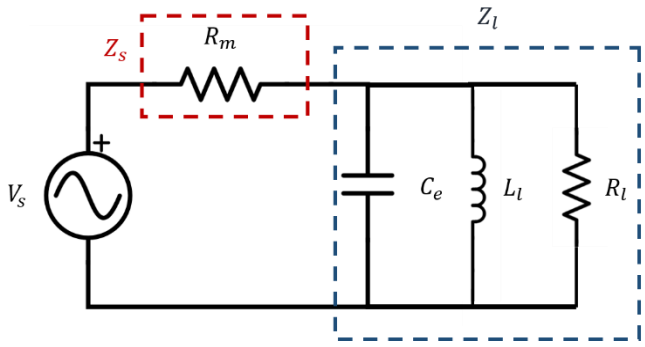

Figure 23 Equivalent circuit at series resonance and connected to the matching load

For the maximum power transfer theorem $Z_l = Z_s^*$, also equal to $Y_l = \frac{1}{Z_s^*}$, where Y_l is the admittance of the load. In general, $Y_l = G_l + jB_l$ and $Z_s = R_s + jX_s$, which yields to the following equation:

$$G_l + jB_l = \frac{1}{R_s - jX_s} \tag{9.5}$$

Equation (9.5) can be separated in the following two terms:

$$G_l = \frac{R_s}{R_s^2 + X_s^2} \quad \Lambda \quad B_l = \frac{X_s}{R_s^2 + X_s^2} \tag{9.6}$$

Moreover, when the CMUT is operated at its resonance frequency, the four components of the source and load impedances have the following values:

$$\begin{aligned} R_s &= R_m \\ X_s &= 0 \\ G_l &= \frac{1}{R_l} \\ B_l &= \omega_{res} C_e - \frac{1}{\omega_{res} L_l} \end{aligned} \tag{9.7}$$

Substituting the values listed in (9.7), the solution to (9.6) is found. This result gives the values of the components to be connected at the load to have the maximum output power, which are:

$$\begin{aligned} R_l &= R_m \\ L_l &= \frac{1}{\omega_{res}^2 C_e} \end{aligned} \tag{9.8}$$

Equation (9.8) shows that the value of the inductor is not unique and it depends on the resonance frequency of the CMUT, therefore it was chosen accordingly.

9.5 Experimental setup

To test the power transfer efficiency of the CMUTs, an experimental setup was built as schematised in Figure 24. The CMUTs, mounted on a PCB, were operated in receiving mode and immersed in a water tank facing a piezoelectric transducer (PZT), used to generate the acoustic waves. The piezoelectric transducer was driven by a function generator (33250A, Agilent Technologies, US) operated in burst mode with a pulse repetition frequency of 10Hz and ten cycles per burst, and whose output signal was amplified using a power amplifier (2100L, Electronics & Innovation Ltd.).

Two PZT devices were used for this experiment (V106 & A120S, Olympus Panametrics NTD), both unfocussed. However, due to the geometry of the transducer a natural focus exists which is located at the Rayleigh distance [63]. The CMUT and the PZT were therefore placed at this distance in order for the CMUT to be in the focus point and receive the maximum pressure generated by the PZT.

The distance was determined by sending ultrasound waves in burst mode with a small number of cycles from the PZT and being received by the CMUTs. Their propagation time was used to define the distance between the transducer and the CMUTs based on the speed of sound in water at ambient temperature. The height and lateral position were adjusted using a manual 3-axis manipulator until the output signal was maximised. The matching load was connected in parallel to the CMUT and its output was monitored with an oscilloscope (MSO6054A, Agilent Technologies, US).

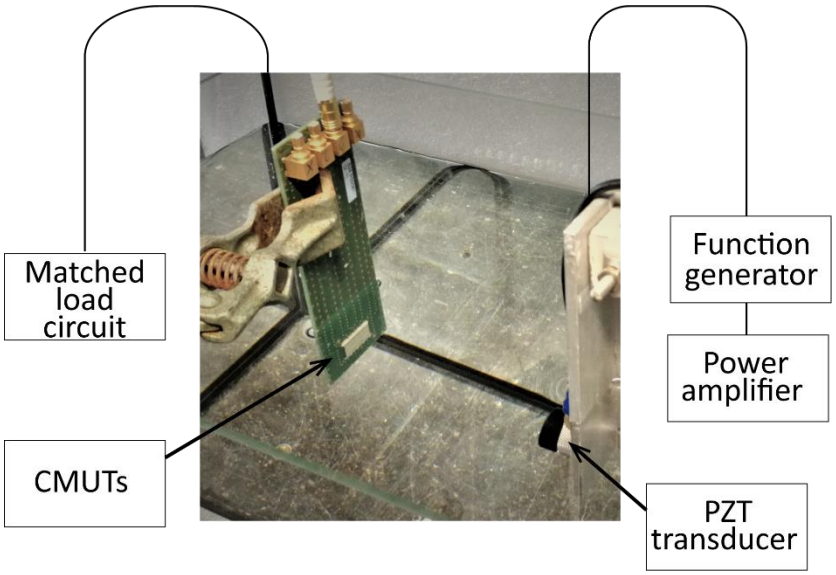

Figure 24 Schematic of the experimental setup

10 Results

10.1 Impedance measurement and parameters extraction

CMUT devices were charged as described in the previous chapter. Their impedance spectrum was then measured in air using an impedance analyser (Agilent 4294A Precision Impedance Analyser). The impedance of an uncharged device with the same structure was also measured at different bias voltages, whose real part is depicted in Figure 25. Specifically, Figure 25.A depicts the spectrum when biased from 60 to 120V, while Figure 25.B from 130 to 170V. it can be seen that the position of the resonance peaks shifts to higher frequencies as the applied bias voltage is increased.

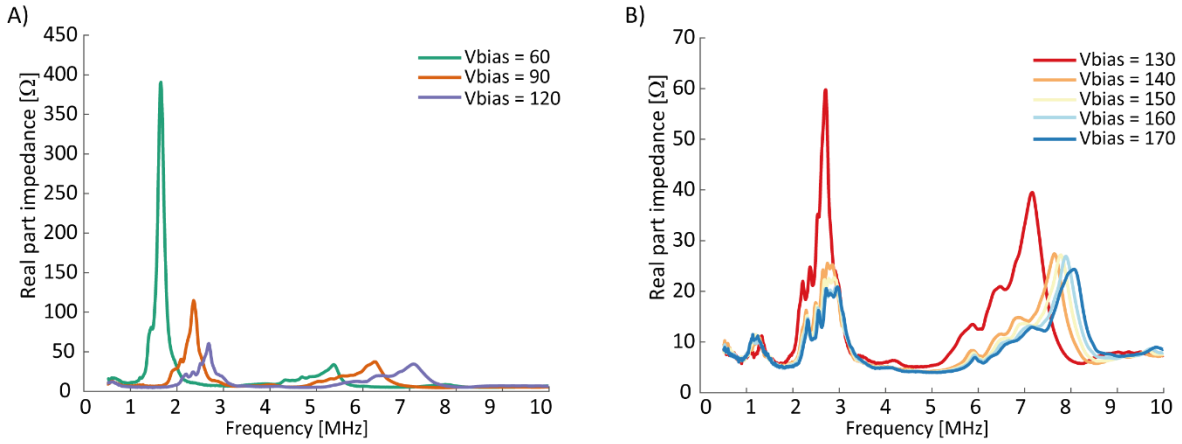

Figure 25 Real part of the impedance spectrum of uncharged CMUTs biased at different voltages. A) Bias voltages from 60 to 120V; B) from 130V to 170V.

The impedance spectrum of the devices with charges trapped in the dielectric is depicted in Figure 26.A, showing two main resonance peaks, as for the uncharged devices, at 5.85MHz and 2.15MHz respectively. The data from the measurements were processed in MatLab and the parameters of the equivalent electrical model extrapolated according to eq. (9.4). Since two resonance peaks are present, two sets of components values, shown in Table 7, were extracted to fit each of the two peaks.

Table 7 Extrapolated components values

f_{res} [MHz]	R_m [Ω]	L_m [μH]	C_m [pF]	C_e [pF]	L_l [μH]
5.85	27.0	13.2	46.7	465.0	1.3
2.15	51.1	146.0	28.8	460.0	9.1

The simulation of the frequency response obtained from the extracted values was then compared to the real impedance spectrum (Figure 26.B-C). The results were then used to define the matching load. However, only the inductor value could be determined, reported in Table 7. The load resistor R_l could not be defined because the impedance of the CMUTs was measured in air while the experiment was done in water. Thus, to obtain the maximum output power, the optimal value for the load resistance was found using a potentiometer.

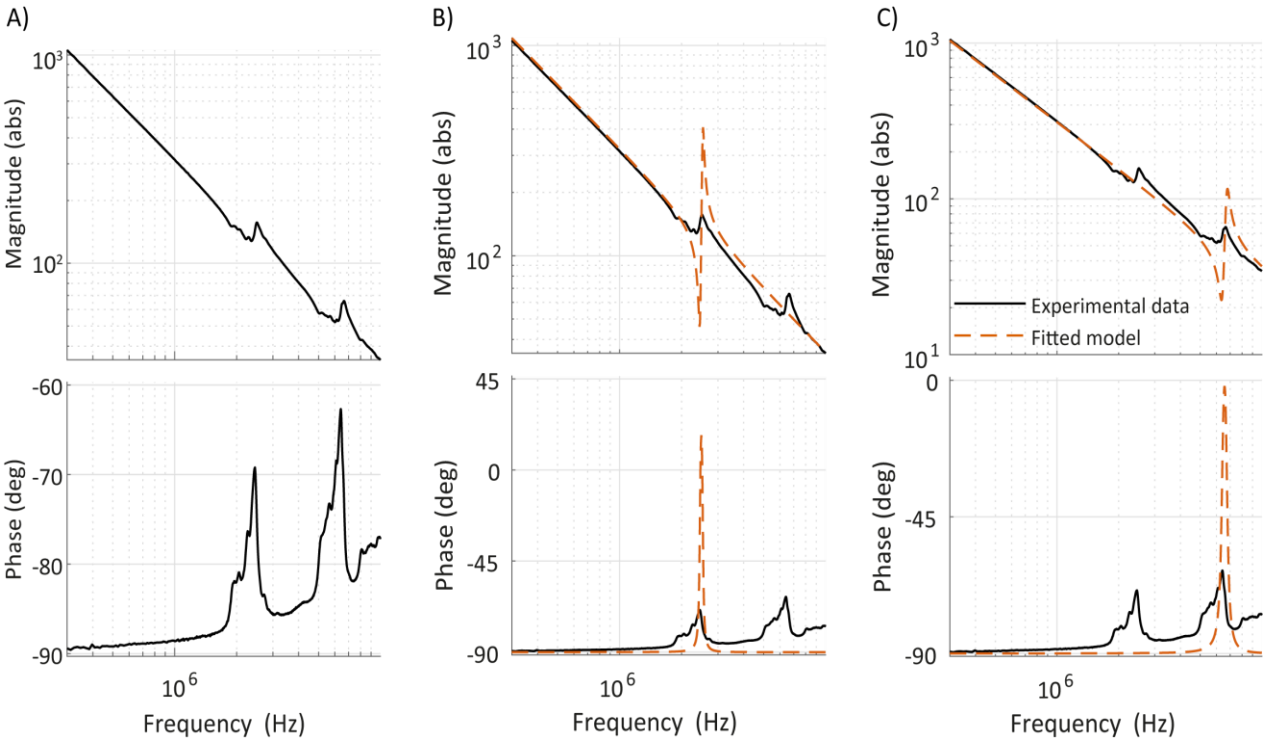

Figure 26 A) Impedance spectrum of charged CMUT. B) Fitting of the model computed from the extracted parameters for 2.15 MHz resonance frequency. B) Same as A) but for 5.85 MHz resonance frequency.

10.2 Estimation of trapped charges

The amount of charges trapped in the Al_2O_3 layer, the frequency response of the charged CMUTs was compared to the one of an uncharged device, biased at different voltages. Figure 27.A shows the comparison between the impedance spectrums of the charged and uncharged CMUTs biased at 100V and 110V. Because of the similarity of the impedance spectrum between the two types of devices, it can be inferred that the equivalent of DC bias voltage of about 110V was stored.

10.3 CMUT power transfer

Due to the fact that the CMUT used in this work has two resonance peaks, two piezoelectric transducers were used, each operated at the closest CMUT resonance frequency. The 2.25MHz transducer was operated at 2.15Mz while the 7.5MHz at 5.85MHz. The output peak-to-peak voltage was recorded with an oscilloscope and the output power (Figure 27.B) was calculated according to the following formula:

$$P_{out} = \frac{V_{pp}^2}{8 \cdot R_l} \tag{10.1}$$

R_l was swept between a range of values using a potentiometer. At 5.85MHz and with a load of 135Ω, the maximum power obtained was 805μW, while at 2.15MHz and 1640Ω the highest value obtained was 423μW.

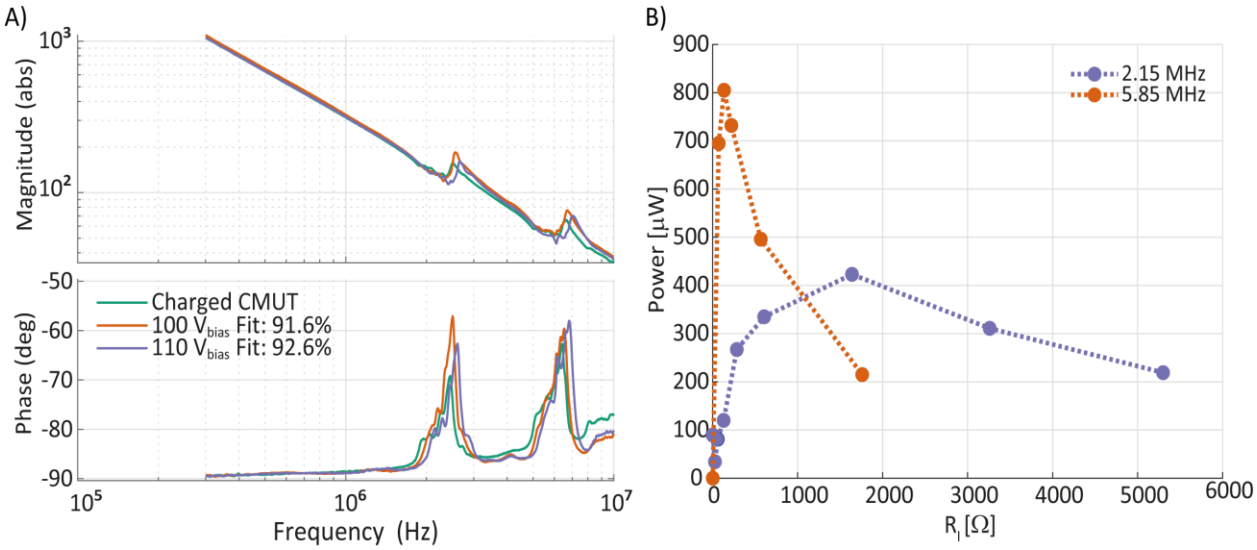

Figure 27 A) Comparison of impedance spectrum to determine the equivalent built-in bias voltage. B) Output power with respect to load resistance for the two resonance frequencies.

10.4 CMUT energy harvesting to power an LED

In addition to the measurement of the output power, to show the potentials of this wireless power transfer method, a second experiment was performed in which an LED was lighted up using the power harvested by the CMUTs. In this case, the CMUTs were operated at 5.85 MHz resonant frequency and the output connected to a load composed of the matching inductor L_l and, instead of the resistor R_l, a voltage quadrupler circuit and a green LED, as in Figure 28.A. In addition, the CMUT devices and the PZT transducer were moved apart, up to a distance of about 80 cm from each other and also at this distance the LED was emitting light. Figure 28.B-C shows the experimental setup with a close view of the CMUTs and the connected load.

10.5 Incoming pressure force

In order to evaluate the power transfer efficiency of the CMUTs, the pressure generated by the two PZTs was measured with a hydrophone (Precision Acoustics 0.5mm needle hydrophone), as described in Appendix A. The pressure profile was measured at the same distance at which the CMUTs and the PZT were placed during the power transfer experiment. A relation exists between acoustic intensity (*I*) and the peak-to-peak pressure (p_{pp}), which depends on the acoustic medium and it is expressed by the following formula:

$$I = \frac{p_{pp}^2}{8 \cdot Z} \tag{10.2}$$

where *Z* is the acoustic impedance of the medium, in this case water. The pressure profile was measured at 2.15MHz at a distance of 70.4mm, and the one at 5.85MHz at a distance of 176mm, which are the respective Rayleigh distances for the two PZTs. The intensity was then calculated according to (10.2) and it is shown in Figure 28. In the two images, yellow represents the highest value and blue the lowest. The 3D profile of the intensity is projected to the bottom of the pictures, on top of which the CMUTs layout on which the intensity is acting is drawn in red.

A)

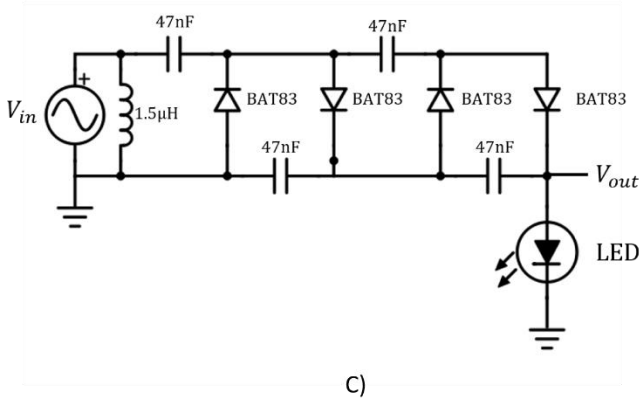

B)

C)

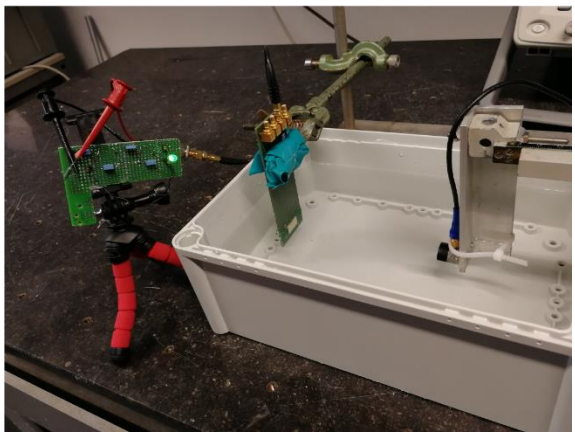

Figure 28 A) Schematic of the load connected to the CMUTs in order to light up a green LED B) Experimental setup of the LED demo; B) Close view of the CMUTs and the PZT. In addition, the load with a green LED emitting light.

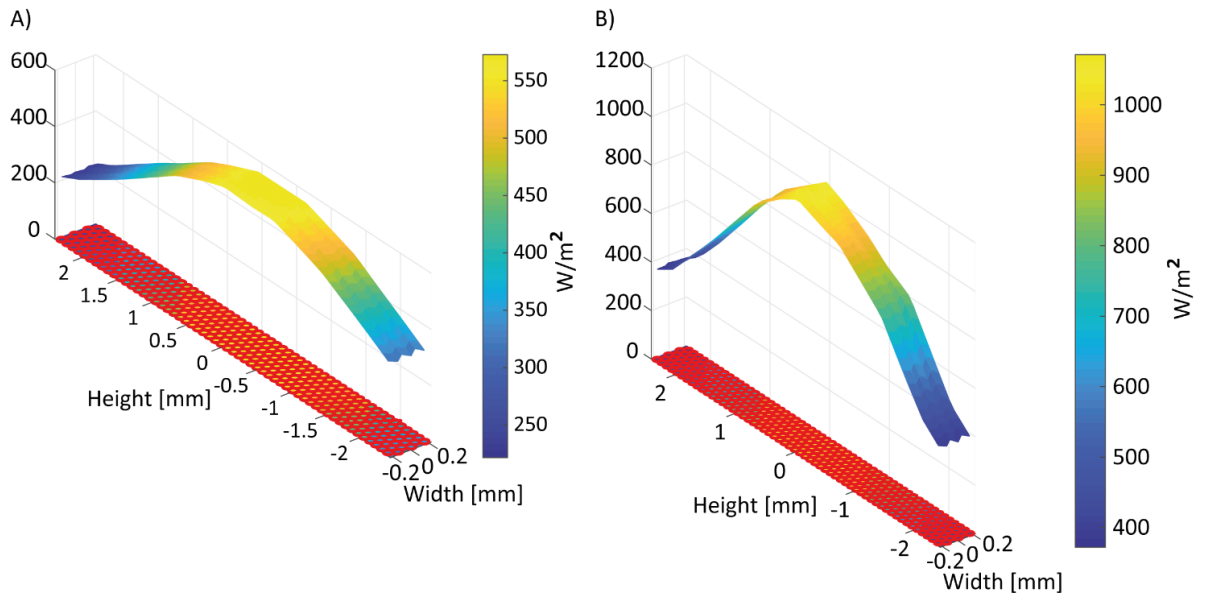

Figure 29 Intensity measured at the two resonance frequencies: A) 2.15MHz, B) 5.85MHz. On the bottom, in red, the layout of the CMUTs arrangement.

10.6 Power transfer efficiency

To calculate the power transfer efficiency, the average intensity acting on the surface of the CMUTs was considered. The relation between intensity and power is expressed by:

$$P = I \cdot A \tag{10.3}$$

Where A is the area of interest, which in this case was approximated with a rectangle of the same dimensions of the area occupied by the CMUTs. The maximum power transfer efficiency was calculated dividing the power generated by the CMUTs by the average of the total incoming power generated by the PZT. Table 8 summarises the results obtained for the two resonance frequencies in which *Average input power* is the average of the power obtained from the pressure profile measurements.

Table 8 Power transfer efficiency results

Frequency [MHz]	Max harvested power [μW]	Average input power [μW]	Average pressure hydrophone [kPa]	Efficiency
2.15	423	975	33.6	43.4%
5.85	805	1650	42.9	48.8%

The maximum efficiency obtained by other groups of researchers which investigated ultrasound power transfer using piezoelectric transducers was in the same order of magnitude. Two representative results are an efficiency of 50%, obtained for a transmitting frequency of 1.2 MHz in water [64] and 39.1% in soft tissue at a depth of 5mm and for a frequency value of 650 kHz [65].

In addition, the spatial-peak pulse-average intensity (I_{SPPA}) was calculated to estimate the feasibility of this power transfer methods and relative parameters. For the frequency 2.15 MHz and 5.85 MHz I_{SPPA} values were respectively 56.5 mW/cm^2 and 106.1 mW/cm^2, therefore both below the safety limit of 190 W/cm^2 set by FDA.

11 Discussion

In this work, CMUTs were used to harvest power generated by an external source. The CMUTs were biased at a high voltage to trap charges in their dielectric. To determine the amount of voltage stored, the impedance spectrum of uncharged CMUTs biased at different voltages was compared to the one of the charged devices. A match of 92.6% was found between the charged devices and the uncharged CMUTs biased at 110V. Hence, it is estimated that this amount of charge was stored in the devices after three hours of charging at 200 V. Moreover, the frequency response of both the charged CMUTs and uncharged ones but biased up to 120V (Figure 25.A and Figure 26) shows two resonance peaks, one at 2.15MHz and the other one at 5.85MHz. Furthermore, increasing the bias voltage three resonance peaks appeared in the spectrum (Figure 25.B), the first at around 1.2MHz, the second at 2.6MHz and the third one at 7.8MHz. Usually a CMUTs have only one resonance peak whose position depends on the voltage at which is biased. The reason of the presence of more than one peak, is that the membrane of these devices resonates at higher order harmonics. In Figure 25.A, the higher resonance frequency is around three times the lower one, therefore it is assumed that the two peaks represent the vibration of the membrane at the first and third order harmonic. In Figure 25.B, the peak at 2.6MHz and the one at 7.8MHz are assumed to represent the vibration of the membrane at the second and sixth order harmonic.

The results of the experiment show a maximum generated output power of 805μW at 5.85MHz and 423μW at 2.15MHz. Considering that the power requirement for an implantable biomedical device is in the range of μW to few mW [45], the energy generated in this case is rather high and can be considered suitable to power an IMD. During the experiment, the resistance at the load was swept in a range of values. However, in Figure 27.B the data points are not evenly spaced because the potentiometer used in the experiment had a coarse regulation system not allowing to step at closer values. However, the error in the determination of the resistance at which the power is the maximum could have been of maximum hundreds of Ohm. In addition, the value of the resistance was measured each time with a multimeter, which might represent another source of error. Nevertheless, these inaccuracies would not cause a large variation in the calculation of the generated power.

The power transfer efficiency at 2.15MHz is 43.4% while at 5.85MHz is 48.8%. Considering that the maximum efficiency that can be reached is 50%, these results are quite outstanding. Moreover, although the CMUTs are packed closely, some space between them is empty and does not contribute to the generation of power. Also, during operation only a ring out of the entire membrane of the CMUTs vibrate which must be considered in the amount of dead area. Furthermore, a possible imperfect match of the connected load, due to the lack of components of the exact value and small inaccuracies in the value of the extracted parameters from the impedance spectrum, contributed to efficiency loss. In addition, the pressure profile measured by the hydrophone needle has an uncertainty of ±9% for the frequencies considered in this work and only the peak-to-peak value out of the entire signal was considered. However, this corresponds to a maximum error of 4% in the efficiency calculation. In addition, measuring the pressure profile with a hydrophone does not take into account the reflections of the acoustic waves hitting the surrounding PCB on which the CMUTs are mounted. These reflections can cause interference and modify the pressure field seen by the CMUTs and this could especially happen if the alignment between the two devices is not perfect. Moreover, a small tilt of the PZT has a large influence on the pressure field seen by a receiver; however, this condition could not be controlled accurately in the experimental setup and during the pressure profile measurement. Also, the output pressure of the PZT is highly dependent on

the temperature of its crystal. This cause a shift in the centre frequency of the transducer which in turn influence its generated pressure. These conditions are likely to have happened, however their effect in the calculation of the efficiency of the power transfer could not be considered since these variables were not measurable in the experimental setup used in this work. A more reliable method is therefore necessary to calculate the power delivered by the PZT to the CMUTs and to obtain a more accurate value of efficiency.

12 Conclusion

Ultrasound as a means of power transfer offers a lot of advantages compared to inductive coupling and radio frequency. In this work, CMUT devices were used as a receiver, instead of the conventional piezoelectric transducers. The need for an external DC bias source was solved using CMUTs with a modified structure. Specifically, the dielectric layer was composed of a stack of $SiO_2/Al_2O_3/SiO_2$. Charges were permanently trapped in the Al_2O_3 layer by applying a large DC bias. A load was powered by the energy harvested by the charged CMUTs without any extra component or equipment. An external pressure source was used to displace the membrane of the devices, operated in receiving mode, with a high efficiency, in line with the state of the art of ultrasonic power transfer using piezoelectric transducers. The corresponding intensity values were also below the safety limits imposed by the FDA for ultrasound imaging. Further optimisation of the experimental setup and of the analysis of the experimental data is necessary, nevertheless the results show that these devices have a great potential for powering an implantable biomedical device, potentially overcoming their need of battery substitution.

12.1 Future work

Due to lack of time, different things were left as a future development:

- Calculate the generated output power considering not only the peak-to-peak value but the entire output signal. Also for the incoming pressure wave, the entire input signal and not only the peak-to-peak value should be considered, in order to calculate the efficiency more precisely.
- Measure the impedance spectrum more precisely to detect the resonance frequency more accurately.
- Build a model for CMUTs with charges trapped in its dielectric.
- Improve the calculation of the incoming pressure force using a method more reliable than the measurement of the pressure profile with a hydrophone needle.
- Determine if, in the human body, the amount of energy which is transferred from the PZT to the CMUTs would still be enough to power an implantable device, considering all the limitations of absorption, therefore attenuation, and heat production.
- Improve the experimental setup to better control the alignment between CMUTs and PZT.

Eventually, the CMUTs used in this work were not fabricated for the purpose of this project, therefore a new design, maybe with different dielectric layer thicknesses, a different dielectric material other than Al_2O_3, membrane stiffness and a closer packing of the devices could give a better efficiency.

13 General conclusion

Ultrasound finds application in many fields, among which the neuromodulation of the nervous system and as a means of power transfer, both are investigated in this thesis. In particular, this thesis demonstrates that high frequency ultrasound is able to both stimulate and inhibit the activity of the nervous system in a reversible way. The effects were tested on healthy and epileptic neurons, both showing a strong response when exposed to ultrasound.

Ultrasound is also an efficient method to transfer power. CMUT devices were used in this thesis which do not require a DC bias source. This was possible using CMUT devices with an Al_2O_3 layer inside the dielectric able to permanently trap charges. Their power transfer efficiency was also estimated, reaching values higher than 48%.

In conclusion, the results obtained from these two experiments pave the way for the deployment of CMUT devices to be implanted inside the body for both the treatment of neurological disorders as well as a wireless power source, highlighting their great potentials in the field of bioelectronic medicine.

APPENDICES

A. Pressure measurement setup

The pressure profiles of the piezoelectric transducers used for the neuromodulation of the neurons and for the CMUT power transfer experiments were both measured by a hydrophone. The measurement setup is depicted in Figure 30.A. A fibre optic (Precision Acoustic, UK) was used giving its adequate sensitivity at the relative low operation frequencies of the transducers. The fibre optic was mounted on a translational stage controlled x-y-z positioning system and operated through the corresponding fibre readout unit. The transducers were fixed on a custom holder and driven by a sine wave generated by function generator and amplified by a power amplifier. Both the transducers and the fibre optic were immersed in a water tank filled with degassed water, aligning the fibre optic to the centre of the transducers (Figure 30.B).

A)

B)

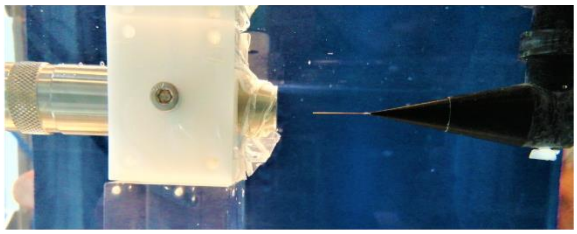

Figure 30 Pressure measurement setup. A) Complete setup: low-right corner water tank for the measurement of the pressure profile on top of which a black structure is the positioning system of the hydrophone; top right the fibre readout unit connected to the oscilloscope (black device under the computer monitor); the function generator is placed under the oscilloscope. B) Detail of the transducer and fibre optic in the water tank.

A computer running a LabVIEW application controlled the movements of the positioning system, triggered the function generator and the fibre readout unit, and the recording of the signal from the fibre readout unit. The fibre optic was only moved on a plane parallel to the face of the ultrasound transducer, scanning the area of interest. For each given position, the recorded signal was averaged to lower the noise level.

Offline data processing of the recorded signal was done in Matlab using a custom made script. Instantaneous pressure values were calculated dividing the recorded signal by the needle sensitivity at the corresponding frequency. The average peak-to-peak pressure amplitude was considered to calculate the intensity.

In addition, to evaluate instantaneous intensity in neuromodulation, spatial-peak pulse average intensity (I_{SPPA}) and pulse-peak temporal average intensities (I_{SPTA}) are typically calculated and they are defined as follows:

$$I_{SPPA} = PII \cdot PRF$$

$$I_{SPTA} = PII \cdot DC$$

Where PII is the pulse intensity integral defined as:

$$PII = \int_{t_1}^{t_2} \frac{p_i^2}{\rho \cdot c} dt$$

Where p_i is the instantaneous pressure amplitude, ρ and *c* are respectively the density and the speed of sound in the medium.

B. Definitions of variables and algorithms for data processing

Spike detection based on differential threshold

The amplitude of the spikes in the recorded extracellular signals was much higher than the background noise, therefore no filtering was applied. Spikes were detected using an algorithm based on a differential threshold. The algorithm was implemented in Matlab based on the work done by Maccione et al. [29]. The differential threshold is set as a multiple of the standard deviation of the biological noise. In this theses

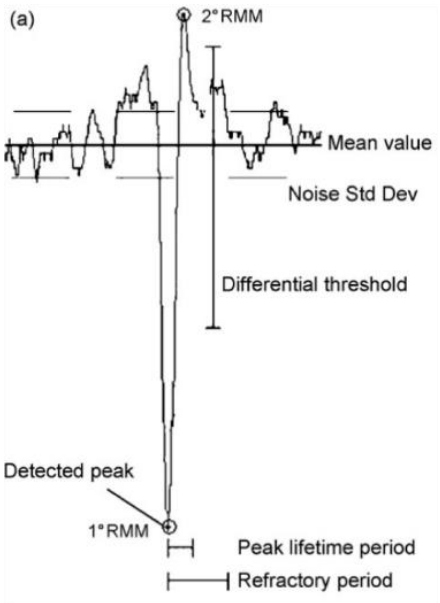

Figure 31 Schematic representation of the spike detection algorithm based on differential threshold. Figure adapted from [29].

7*SD was chosen as differential threshold. A time window is also set which is the maximum possible duration of a spike, named peak lifetime period (PLP). The relative minimum and maximum of the recorded signal are then computed. When a relative minimum or maximum is detected, the next one in searched in the PLP window. If the difference in amplitude between the two detected peaks overcome the differential threshold, a spike is identified. In addition, a refractory period is set. After a spike is detected, no other spikes can be detected within the refractory period time window. Peak lifetime period and refractory period were set to 2 ms and 2.5 ms respectively. A schematic representation is depicted in Figure 31.

Burst detection algorithm

Bursts are defined as a sequence of closely spaced spikes. The burst detection algorithm was written based on the steps reported in the Multiwell-MEA-System Manual (Multichannel systems, Germany) [66] and reported in the following.

- The spike train is scanned until an inter-spike interval is found that is less than or equal to *max interval,* here set to 50 ms
- While the inter-spike interval is less than *max inter-spike interval*, spikes are included in the burst. *Max inter-spike interval* was set to 50 ms
- If the inter-spike interval is more than *max inter-spike interval*, the burst ends.
- If the distance between consecutive detected bursts is less than *min interval between bursts*, the bursts are merged together. *Min interval between bursts* was set to 100 ms
- All the bursts that have fewer spikes than *min number of spikes* are removed, here set to 10 spikes.

The defined variables are depicted in Figure 32.

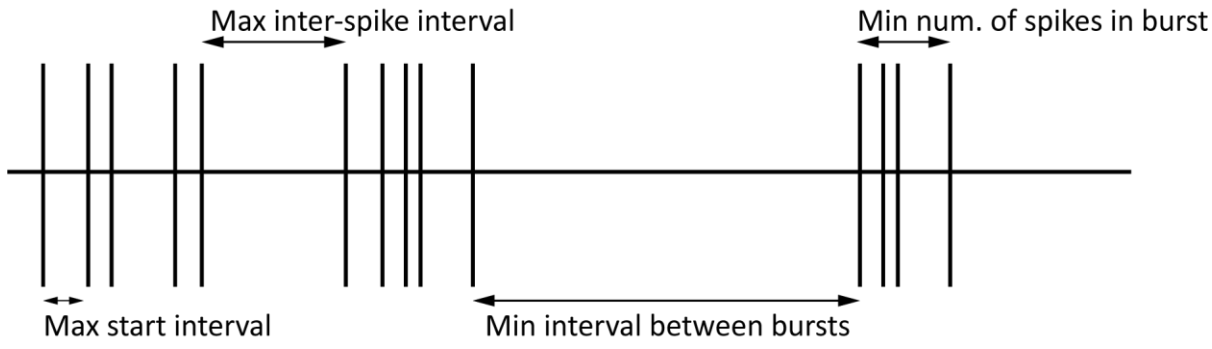

Figure 32 Burst detection algorithm variables

C. Design of the components of the neuromodulation experiment

In order to allow the ultrasound transducers to be placed inside the wells of the MEA, a new lid to cover the MEA headstage was designed. Components of the lid and the supports for the ultrasound transducers were designed in Solidworks based on the idea of a puzzle, to allow an easy assembly. They were then lasercut from a piece of transparent acrylic material of thickness 3 mm or 5 mm depending on the specific piece of the assembly. Afterwards, they were glued together. The support used to ensure a stable position of the MEA headstage with respect to the lid were also designed in Solidworks and fabricated in Aluminium in the mechanics workshop of Philips Research. The complete assembly and the detailed view of each subassembly of the setup are shown in the following pictures.

A) Complete assembly

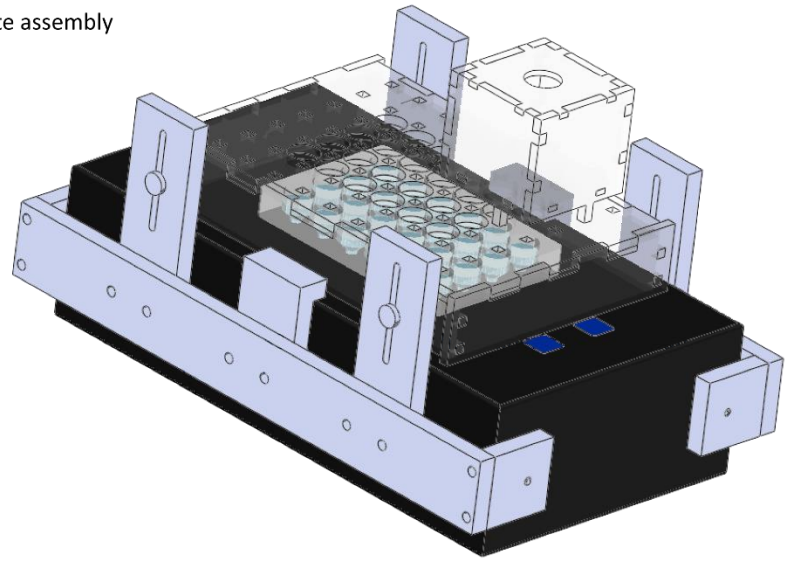

B) Aluminium support and its exploded view

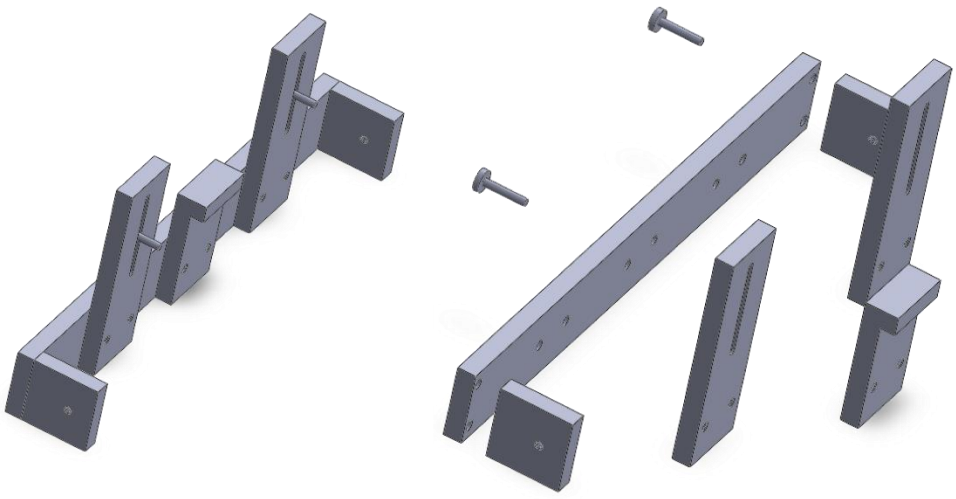

C) Lid for the MEA headstage and its exploded view

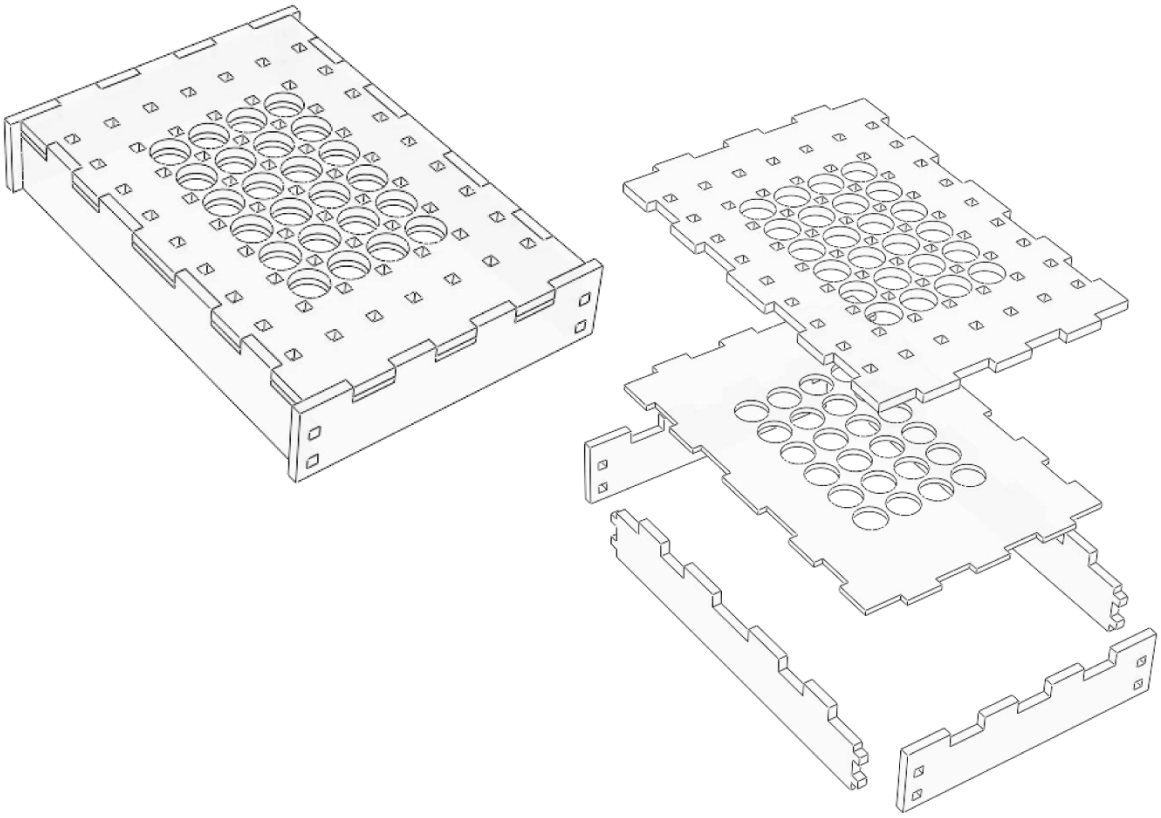

D) Support for the ultrasound transducer and its exploded view. Its legs fit in the holes engraved on the MEA lid to allow easy and stable positioning

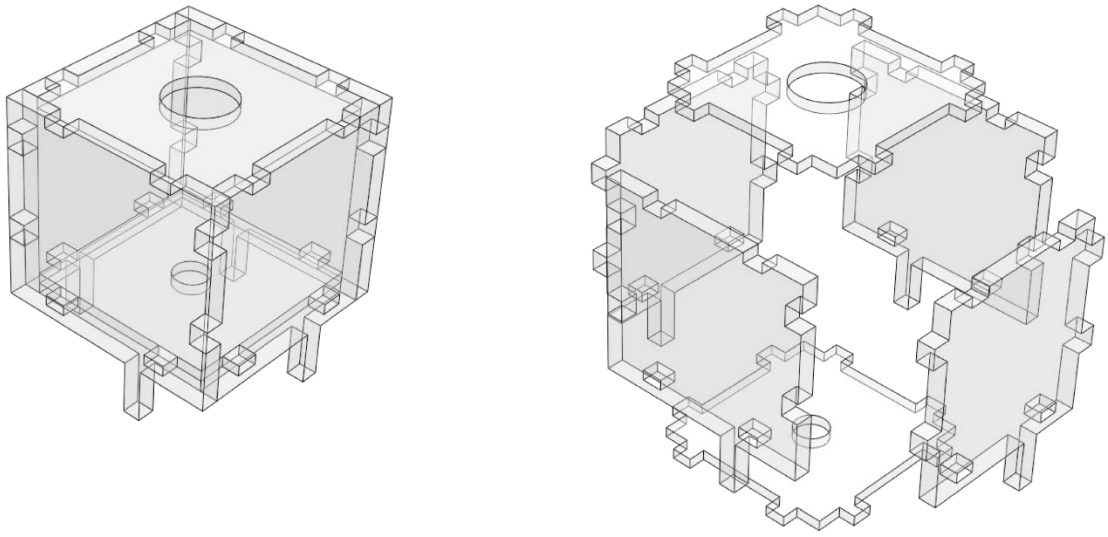

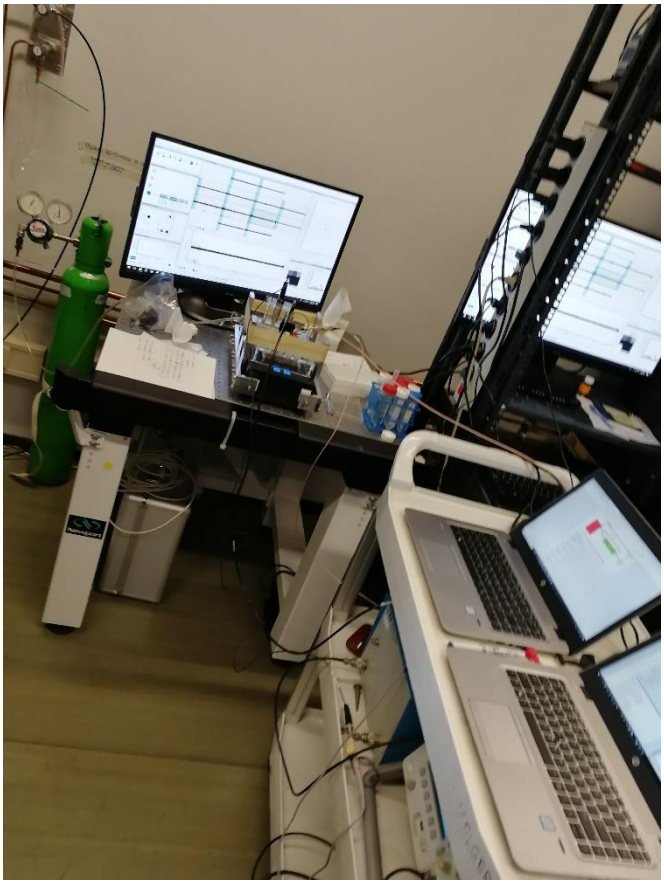

Figure 34 Complete experimental setup at Erasmus MC

Table 9 Summary of sonication parameters used in stimulation studies

Author Year	Frequency [MHz]	Isppa [W/cm2]	Ispta [W/cm2]	TBD(s)	Tus stim [s]	c/tb	Ntb	PRF [Hz]	DC	burst/CW	Study	Measurement method	Temperature elevation	Peak pressure [MPa]	focus
Tyler 2008 [15]	0.44 - 0.67	2.90	2.3e-2 - 2.16	1.8e-4 - 7.4e-2	0.3 – 0.5	80 – 5e+5	3 - 5	10	0.1 – 74.5	burst	*in vitro* CA1 hippocampus of mice	Whole cell current clamp recording		<1	
Muratore 2009 [67]	4.04	0.19	0.19	1.0e-4	1.0e-4				100	CW	*in vitro* hippocampus of rats	Microelectrode array		7.7e-2	
Vykhodtseva 2006 [68]	4.6	153	76	0.01-0.1	10-40	4.6e+4 - 5.0e+5	50-400	5-10	5-100	burst	*in vivo* hippocampus and thalamus of rats	Electrodes		0.9-3.5	Not stated
Kim 2019 [69]	0.183	0.53	4.7e-2	4.5e-3	0.2	756	40	200	90	burst	*in vivo* motor cortex of mice	EMG		0.05	2.75mm
Lin 2018 [70]	27.38	0.85-3.14-3.66-5.13	0.85-3.14-3.66-5.13		30				100	CW	*in vitro* hippocampus of rats	Patch clamp	5	0.13-0.25-0.27-0.32	Not stated
Yoo 2011 [37]	0.69	3.3	1.6	5.0e-2	1	3.5e+4	10	10	50	burst	*in vivo* motor cortex of rabbits	EEG			2.3mm
Tufail 2010 [7]	0.25-0.5	0.07-0.23	0.02-0.16	1.6e-4 - 5.7e-4	0.03-0.33	80-225		1200-3000		burst	*in vivo* motor cortex and hippocampi of mice	Microelectrode and EMG	<0.01	0.07-0.1	2 to 4.7mm
Prieto 2018 [71]	43	50-90	50-90		1				100	CW	*in vitro* rat and mice excitable cells	Patch clamp			90μm
Kim 2014 [72]	0.35	different	different	0.25 to 5	0.2 - 0.3 - 0.4			100 to 2000	30-50-70	burst	*in vivo* motor cortex of rats	Visual	0.97		

Author Year	Frequency [MHz]	Isppa [W/cm2]	Ispta [W/cm2]	TBD(s)	Tus stim [s]	c/tb	Ntb	PRF [Hz]	DC	burst/CW	Study	Measurement method	Temperature elevation	Peak pressure [MPa]	focus
Han 2018 [25]	0.35	3.36	1.16	2.3e-4	6.7e-2	80	100	1500	34.5	burst	*in vivo* and *in vitro* motor cortex of mice	Video recording for *in vivo* and calcium imaging for *in vitro*	Not stated	0.06	6.6mm
Li 2016 [73]	5	0.26 to 0.46	0.13 to 0.23	5.0e-4	60	2500	6.0e+4	1000	50	burst	*in vivo* close to bregma of mice	EMG	1.6		0.86mm
Kim 2017 [74]	0.5	7.8e-4	1.9e-6	2.1e-6	180	1	2.1e+5	1160	0.24	burst	*in vitro* hippocampus of rats	MEA	No	1.2e-2	unfocused
Khraiche 2008 [75]	7.75		50-150	1.0e-3	60	7750	120	2	0.2	burst	*in vitro* hippocampus of rats	MEA	0.004		
Kim 2015 [39]	0.35	3-5	0.25	5.0e-4	150	175	1.5e+4	100	8.3 - 5	burst	*in vivo* visual cortex of rats	EEG	Not stated		3.7mm
King 2013 [24]	0.25 to 0.6		0.01 to 79.02		0.02 to 0.48			11 to 3000	100 and lower	CW and burst	*in vivo* mice	EMG		0.03 to 1.11	
Fisher 2018 [76]	0.51	0.69	0.34	5.0e-4	1	255	1000	1000	50	burst	*in vivo* primary somatosensory cortex of mice	Optical imaging	Not stated	0.17	3.3mm
Younan 2013 [18]	0.32	17.5	8.05	2.3e-4	0.25	75	500	2000	50	burst	*in vivo* different brain areas of rats	EMG and visual	Not stated	0.4 to 1	Not stated
Lee 2016 [77]	0.25	11.8 – 14.3	5.9 – 7.15	1.0e-3	0.3	250	150	500	50	burst	*in vivo* primary sensorymotor cortex of sheep	EMG	0.04		7mm

Table 10 Summary of sonication parameters used in inhibition studies

Author Year	Frequency [MHz]	Isppa [W/cm2]	Ispta [W/cm2]	TBD(s)	Tus stim [s]	c/tb	Ntb	PRF [Hz]	DC	Burst/CW	Study	Measurement method	Temperature elevation	Peak pressure [MPa]	focus
Rinaldi 1991 [36]	0.75	91.1	82	6.0e-6	180 to 900	4	2.7e+7 to 1.35e+8	1.5E+5	90	burst	*in vitro* hippocampus of rats	Microelectrodes	0.8	Not stated	1mm
Yoo 2011 [37]	0.69	3.3	0.16	5.0e-4	7-8	345	700-800	100	5	burst	*in vivo* visual cortex of rabbits	EEG (subdermal electrodes)	No		2.3mm
Min 2011 [38]	0.69	2.6	0.13	5.0e-4	180	345	1.8e+5	100	5	burst	*in vivo* PTZ induced epilepsy in rats thalamus	EEG		0.27	3.5mm
Hakimova 2015 [78]	0.2	Not specified	Not specified	1e-3	30	200	1.5e+4	500	50	burst	*in vivo* KA induced epilepsy in mice hippocampus	EEG			Unfocused
Kim 2015 [39]	0.35	3	0.15	5.0e-4	150	175	1.5e+4	100	5	burst	*in vivo* visual cortex of rats	EEG (subdermal electrodes)			3.7mm
Gulick 2017 [79]	0.2	200	100	5.0e-4	0.3	100		0.5	50	burst	*in vivo* motor cortex of rats	EMG	3		3.5mm
Yoo 2010 [80]	0.69	50	25	5.0e-3	60	3450	6e+3	100	50	burst	*in vivo* KA induced epilepsy in rats hippocampus	EEG (subdermal electrodes)	No		
Daniels 2018 [40]	0.23	2.3-4.6	0.07-0.15	0.1	52	2.3e+4	17	0.33	3	burst	*in vivo* inferior colliculus of rats and auditory cortex of pigs	EEG	No	0.0397-0.0793	3mm
Fry 1950 [81]	0.98	35	35		43.5				100	CW	*in vitro* ventral nerve cord of lobster	Electrodes	1		
Sharabi 2019 [41]	0.23	27.2	0.9	0.1	52	2.3e+4	18	0.33	3.3	pulsed	*In vivo* olivo-cerebellar system of rats	EMG			

Bibliography

[1] D. L. Miller, N. B. Smith, M. R. Bailey, G. J. Czarnota, K. Hynynen, and I. R. S. Makin, "Overview of Therapeutic Ultrasound Applications and Safety Considerations," *J. Ultrasound Med.*, vol. 31, no. 4, pp. 623–634, Apr. 2012.

[2] D.-S. Lin, X. Zhuang, S. H. Wong, M. Kupnik, and B. T. Khuri-Yakub, "Encapsulation of Capacitive Micromachined Ultrasonic Transducers Using Viscoelastic Polymer," *J. Microelectromechanical Syst.*, vol. 19, no. 6, pp. 1341–1351, Dec. 2010.

[3] K. T. Thakur *et al.*, *Disease Control Priorities, Third Edition (Volume 4): Mental, Neurological, and Substance Use Disorders*. The World Bank, 2016.

[4] V. L. Feigin *et al.*, "Global, regional, and national burden of neurological disorders during 1990–2015: a systematic analysis for the Global Burden of Disease Study 2015," *Lancet Neurol.*, vol. 16, no. 11, pp. 877–897, Nov. 2017.

[5] OMS, "Nearly 1 in 6 of world's population suffer from neurological disorders," *Organização Mundial de Saúde*, 2007. [Online]. Available: https://news.un.org/en/story/2007/02/210312-nearly-1-6-worlds-population-suffer-neurological-disorders-un-report. [Accessed: 21-Mar-2019].

[6] O. Naor, S. Krupa, and S. Shoham, "Ultrasonic neuromodulation," *J. Neural Eng.*, vol. 13, no. 3, p. 031003, Jun. 2016.

[7] Y. Tufail *et al.*, "Transcranial Pulsed Ultrasound Stimulates Intact Brain Circuits," *Neuron*, vol. 66, no. 5, pp. 681–694, Jun. 2010.

[8] Y. Tufail, A. Yoshihiro, S. Pati, M. M. Li, and W. J. Tyler, "Ultrasonic neuromodulation by brain stimulation with transcranial ultrasound," *Nat. Protoc.*, vol. 6, no. 9, pp. 1453–1470, Sep. 2011.

[9] E. N. Harvey, "The effect of high frequency sound waves on heart muscle and other irritable tissues," *Am. J. Physiol. Content*, vol. 91, no. 1, pp. 284–290, Dec. 1929.

[10] T. Yang, J. Chen, B. Yan, and D. Zhou, "Transcranial ultrasound stimulation: A possible therapeutic approach to epilepsy," *Med. Hypotheses*, vol. 76, no. 3, pp. 381–383, Mar. 2011.

[11] M. D. Menz, O. Oralkan, P. T. Khuri-Yakub, and S. A. Baccus, "Precise Neural Stimulation in the Retina Using Focused Ultrasound," *J. Neurosci.*, vol. 33, no. 10, pp. 4550–4560, Mar. 2013.

[12] W. D. O'Brien, "Ultrasound-biophysics mechanisms," *Progress in Biophysics and Molecular Biology*, vol. 93, no. 1–3. NIH Public Access, pp. 212–255, 2007.

[13] G. ter Haar, *The Safe Use of Ultrasound in Medical Diagnosis*. 2012.

[14] D. Dalecki, "Mechanical Bioeffects of Ultrasound," *Annu. Rev. Biomed. Eng.*, vol. 6, no. 1, pp. 229–248, Aug. 2004.

[15] W. J. Tyler, Y. Tufail, M. Finsterwald, M. L. Tauchmann, E. J. Olson, and C. Majestic, "Remote Excitation of Neuronal Circuits Using Low-Intensity, Low-Frequency Ultrasound," *PLoS One*, vol. 3, no. 10, p. e3511, Oct. 2008.

[16] M. D. Menz, P. Ye, K. Firouzi, K. B. Pauly, B. T. Khuri-Yakub, and S. A. Baccus, "Physical mechanisms of ultrasonic neurostimulation of the retina," *bioRxiv*, p. 231449, 2017.

[17] H. Baek, K. J. Pahk, and H. Kim, "A review of low-intensity focused ultrasound for neuromodulation," *Biomed. Eng. Lett.*, vol. 7, no. 2, pp. 135–142, May 2017.

[18] Y. Younan, T. Deffieux, B. Larrat, M. Fink, M. Tanter, and J.-F. Aubry, "Influence of the pressure field distribution in transcranial ultrasonic neurostimulation," *Med. Phys.*, vol. 40, no. 8, p. 082902, Jul. 2013.

[19] R. A. Wahab, M. Choi, Y. Liu, V. Krauthamer, V. Zderic, and M. R. Myers, "Mechanical bioeffects of pulsed high intensity focused ultrasound on a simple neural model," *Med. Phys.*, vol. 39, no. 7Part1, pp. 4274–4283, Jun. 2012.

[20] B. Krasovitski, V. Frenkel, S. Shoham, and E. Kimmel, "Intramembrane cavitation as a unifying mechanism for ultrasound-induced bioeffects," *Proc. Natl. Acad. Sci.*, vol. 108, no. 8, pp. 3258–3263, Feb. 2011.

[21] M. Plaksin, S. Shoham, and E. Kimmel, "Intramembrane Cavitation as a Predictive Bio-Piezoelectric Mechanism for Ultrasonic Brain Stimulation," *Phys. Rev. X*, vol. 4, no. 1, p. 011004, Jan. 2014.

[22] M. J. Borrelli, K. I. Bailey, and F. Dunn, "Early ultrasonic effects upon mammalian CNS structures (chemical synapses)," *J. Acoust. Soc. Am.*, vol. 69, no. 5, pp. 1514–1516, May 1981.

[23] R. T. Mihran, F. S. Barnes, and H. Wachtel, "Temporally-specific modification of myelinated axon excitability in vitro following a single ultrasound pulse," *Ultrasound Med. Biol.*, vol. 16, no. 3, pp. 297–309, Jan. 1990.

[24] R. L. King, J. R. Brown, W. T. Newsome, and K. B. Pauly, "Effective Parameters for Ultrasound-Induced In Vivo Neurostimulation," *Ultrasound Med. Biol.*, vol. 39, no. 2, pp. 312–331, Feb. 2013.

[25] S. Han, M. Kim, H. Kim, H. Shin, and I. Youn, "Ketamine Inhibits Ultrasound Stimulation-Induced Neuromodulation by

Blocking Cortical Neuron Activity," *Ultrasound Med. Biol.*, vol. 44, no. 3, pp. 635–646, Mar. 2018.

[26] M. Proietti Onori *et al.*, "The intellectual disability-associated CAMK2G p.Arg292Pro mutation acts as a pathogenic gain-of-function," *Hum. Mutat.*, vol. 39, no. 12, pp. 2008–2024, Dec. 2018.

[27] StemLabs, "Red Pitaya," 2019. [Online]. Available: https://www.redpitaya.com/.

[28] Multi Channel Systems MCS GmbH, "Multichannel system - Software." [Online]. Available: https://www.multichannelsystems.com/products/multiwell-screen#downloads.

[29] A. Maccione, M. Gandolfo, P. Massobrio, A. Novellino, S. Martinoia, and M. Chiappalone, "A novel algorithm for precise identification of spikes in extracellularly recorded neuronal signals," *J. Neurosci. Methods*, vol. 177, no. 1, pp. 241–249, Feb. 2009.

[30] M. Chiappalone, A. Novellino, I. Vajda, A. Vato, S. Martinoia, and J. van Pelt, "Burst detection algorithms for the analysis of spatio-temporal patterns in cortical networks of neurons," *Neurocomputing*, vol. 65–66, pp. 653–662, Jun. 2005.

[31] Statistics How To, "What is Friedman's Test?," 2019. [Online]. Available: https://www.statisticshowto.datasciencecentral.com/friedmans-test/.

[32] N. Salkind, *Encyclopedia of Measurement and Statistics*. 2455 Teller Road, Thousand Oaks California 91320 United States of America: Sage Publications, Inc., 2007.

[33] ITIS Foundation, "Tissue acoustic properties." [Online]. Available: https://itis.swiss/virtual-population/tissue-properties/database/acoustic-properties/attenuation-constant/.

[34] T. A. Bigelow *et al.*, "The Thermal Index," *J. Ultrasound Med.*, vol. 30, no. 5, pp. 714–734, May 2011.

[35] L. Sherwood, *Fundamentals of Human Physiology*. Cengage Learning.

[36] P. C. Rinaldi, J. P. Jones, F. Reines, and L. R. Price, "Modification by focused ultrasound pulses of electrically evoked responses from an in vitro hippocampal preparation," *Brain Res.*, vol. 558, no. 1, pp. 36–42, Aug. 1991.

[37] S.-S. Yoo *et al.*, "Focused ultrasound modulates region-specific brain activity," *Neuroimage*, vol. 56, no. 3, pp. 1267–1275, Jun. 2011.

[38] B.-K. Min *et al.*, "Focused ultrasound-mediated suppression of chemically-induced acute epileptic EEG activity," *BMC Neurosci.*, vol. 12, no. 1, p. 23, 2011.

[39] H. Kim, M. Y. Park, S. D. Lee, W. Lee, A. Chiu, and S.-S. Yoo, "Suppression of EEG visual-evoked potentials in rats through neuromodulatory focused ultrasound," *Neuroreport*, vol. 26, no. 4, pp. 211–215, Mar. 2015.

[40] D. Daniels *et al.*, "Focused Ultrasound-Induced Suppression of Auditory Evoked Potentials in Vivo," *Ultrasound Med. Biol.*, vol. 44, no. 5, pp. 1022–1030, May 2018.

[41] S. Sharabi *et al.*, "Non-thermal focused ultrasound induced reversible reduction of essential tremor in a rat model," *Brain Stimul.*, vol. 12, no. 1, pp. 1–8, Jan. 2019.

[42] S. Mishra, "Electroceuticals in medicine – The brave new future," *Indian Heart J.*, vol. 69, no. 5, pp. 685–686, Sep. 2017.

[43] X. Li, W. A. Serdijn, W. Zheng, Y. Tian, and B. Zhang, "The injectable neurostimulator: an emerging therapeutic device," *Trends Biotechnol.*, vol. 33, no. 7, pp. 388–394, Jul. 2015.

[44] SetPoint Medical, "SetPoint Medical Platform," 2019. [Online]. Available: https://setpointmedical.com/bioelectronic-medicine-therapy/.

[45] A. Ben Amar, A. B. Kouki, and H. Cao, "Power approaches for implantable medical devices," *Sensors (Switzerland)*, vol. 15, no. 11. Multidisciplinary Digital Publishing Institute (MDPI), pp. 28889–28914, 13-Nov-2015.

[46] M. A. Hannan, S. Mutashar, S. A. Samad, and A. Hussain, "Energy harvesting for the implantable biomedical devices: Issues and challenges," *BioMedical Engineering Online*, vol. 13, no. 1. pp. 1–23, 2014.

[47] J. Charthad *et al.*, "A mm-Sized Wireless Implantable Device for Electrical Stimulation of Peripheral Nerves," *IEEE Trans. Biomed. Circuits Syst.*, vol. 12, no. 2, pp. 257–270, Apr. 2018.

[48] E. Waffenschmidt and T. Staring, "Limitation of inductive power transfer for consumer applications," *13th Eur. Conf. Power Electron. Appl.*, 2009.

[49] H. Basaeri, D. B. Christensen, and S. Roundy, "A review of acoustic power transfer for bio-medical implants," *Smart Materials and Structures*, vol. 25, no. 12. IOP Publishing, p. 123001, 01-Dec-2016.

[50] K. Agarwal, R. Jegadeesan, Y.-X. Guo, and N. V. Thakor, "Wireless Power Transfer Strategies for Implantable Bioelectronics," *IEEE Rev. Biomed. Eng.*, vol. 10, pp. 136–161, 2017.

[51] A. Sanni and A. Vilches, "Powering low-power implants using PZT transducer discs operated in the radial mode," *Smart Mater. Struct.*, vol. 22, no. 11, p. 115005, Nov. 2013.

[52] M. S. Salim, M. F. Abd Malek, R. B. W. Heng, K. M. Juni, and N. Sabri, "Capacitive Micromachined Ultrasonic Transducers:

Technology and Application," *J. Med. Ultrasound*, vol. 20, no. 1, pp. 8–31, Mar. 2012.

[53] I. Ladabaum, X. Jin, H. T. Soh, A. Atalar, and B. T. Khuri-Yakub, "Surface micromachined capacitive ultrasonic transducers," *IEEE Trans. Ultrason. Ferroelectr. Freq. Control*, vol. 45, no. 3, pp. 678–690, May 1998.

[54] G. M. Sessler, "Electric fields and forces due to charged dielectrics," *J. Appl. Phys.*, vol. 43, no. 2, pp. 405–408, 1972.

[55] T. Mellow and L. Kärkkäinen, "On the forces in single-ended and push-pull electret transducers.," *J. Acoust. Soc. Am.*, vol. 124, no. 3, pp. 1497–504, 2008.

[56] M. C. Ho, M. Kupnik, K. K. Park, and B. T. Khuri-Yakub, "Long-term measurement results of pre-charged CMUTs with zero external bias operation," in *IEEE International Ultrasonics Symposium, IUS*, 2012, pp. 89–92.

[57] A. Kshirsagar, A. Sampaleanu, R. Chee, W. Moussa, and R. J. Zemp, "Pre-charged CMUTs with efficient low-bias voltage operation for medical applications," in *IEEE International Ultrasonics Symposium, IUS*, 2013, pp. 1728–1730.

[58] F. Y. Lin, W. C. Tian, and P. C. Li, "CMOS-based Capacitive Micromachined Ultrasonic Transducers operating without external DC bias," in *IEEE International Ultrasonics Symposium, IUS*, 2013, pp. 1420–1423.

[59] K. K. Park, M. Kupnik, H. J. Lee, Ö. Oralkan, and B. T. Khuri-Yakub, "Zero-bias resonant sensor with an oxide-nitride layer as charge trap," in *Proceedings of IEEE Sensors*, 2010, pp. 1024–1028.

[60] G. Puzzilli, B. Govoreanu, F. Irrera, M. Rosmeulen, and J. Van Houdt, "Characterization of charge trapping in SiO2/Al2O3 dielectric stacks by pulsed C-V technique," *Microelectron. Reliab.*, vol. 47, no. 4-5 SPEC. ISS., pp. 508–512, 2007.

[61] H. Köymen *et al.*, "An improved lumped element nonlinear circuit model for a circular CMUT cell," *IEEE Trans. Ultrason. Ferroelectr. Freq. Control*, vol. 59, no. 8, pp. 1791–1799, Aug. 2012.

[62] S. Satir, "Modeling and Optimization of Capacitive Micromachined Ultrasonic Transducers," no. December, Nov. 2014.

[63] Panametrics-NDT, "Ultrasonic transducers technical notes." 2017.

[64] Y. Shigeta, Y. Hori, K. Fujimori, K. Tsuruta, and S. Nogi, "Development of highly efficient transducer for wireless power transmission system by ultrasonic," in *2011 IEEE MTT-S International Microwave Workshop Series on Innovative Wireless Power Transmission: Technologies, Systems, and Applications*, 2011, pp. 171–174.

[65] S. Ozeri, D. Shmilovitz, S. Singer, and C.-C. Wang, "Ultrasonic transcutaneous energy transfer using a continuous wave 650kHz Gaussian shaded transmitter," *Ultrasonics*, vol. 50, no. 7, pp. 666–674, Jun. 2010.

[66] Multi Channel Systems MCS GmbH, "Multiwell-MEA Analyzer." [Online]. Available: https://www.multichannelsystems.com/software/multiwell-analyzer#docs.

[67] R. Muratore *et al.*, "Bioeffective Ultrasound at Very Low Doses: Reversible Manipulation of Neuronal Cell Morphology and Function in Vitro," in *AIP Conference Proceedings*, 2009, vol. 1113, pp. 25–29.

[68] N. I. Vykhodtseva, "Steady Potential Changes and Spreading Depression in Rat Brains Produced by Focused Ultrasound," in *AIP Conference Proceedings*, 2006, vol. 829, pp. 59–63.

[69] H. Kim *et al.*, "Miniature ultrasound ring array transducers for transcranial ultrasound neuromodulation of freely-moving small animals," *Brain Stimul.*, vol. 12, no. 2, pp. 251–255, Mar. 2019.

[70] Z. Lin *et al.*, "On-Chip Ultrasound Modulation of Pyramidal Neuronal Activity in Hippocampal Slices," *Adv. Biosyst.*, vol. 2, no. 8, p. 1800041, Aug. 2018.

[71] M. L. Prieto, K. Firouzi, B. T. Khuri-Yakub, and M. Maduke, "Activation of Piezo1 but Not NaV1.2 Channels by Ultrasound at 43 MHz," *Ultrasound Med. Biol.*, vol. 44, no. 6, pp. 1217–1232, Jun. 2018.

[72] H. Kim, A. Chiu, S. D. Lee, K. Fischer, and S.-S. Yoo, "Focused Ultrasound-mediated Non-invasive Brain Stimulation: Examination of Sonication Parameters," *Brain Stimul.*, vol. 7, no. 5, pp. 748–756, Sep. 2014.

[73] G.-F. Li *et al.*, "Improved Anatomical Specificity of Non-invasive Neuro-stimulation by High Frequency (5 MHz) Ultrasound," *Sci. Rep.*, vol. 6, no. 1, p. 24738, Jul. 2016.

[74] H.-B. Kim *et al.*, "Prolonged stimulation with low-intensity ultrasound induces delayed increases in spontaneous hippocampal culture spiking activity," *J. Neurosci. Res.*, vol. 95, no. 3, pp. 885–896, Mar. 2017.

[75] M. L. Khraiche, W. B. Phillips, N. Jackson, and J. Muthuswamy, "Ultrasound induced increase in excitability of single neurons," in *2008 30th Annual International Conference of the IEEE Engineering in Medicine and Biology Society*, 2008, vol. 2008, pp. 4246–4249.

[76] J. A. N. Fisher and I. Gumenchuk, "Low-intensity focused ultrasound alters the latency and spatial patterns of sensory-evoked cortical responses in vivo," *J. Neural Eng.*, vol. 15, no. 3, p. 035004, Jun. 2018.

[77] W. Lee *et al.*, "Image-Guided Focused Ultrasound-Mediated Regional Brain Stimulation in Sheep," *Ultrasound Med. Biol.*, vol. 42, no. 2, pp. 459–470, Feb. 2016.

[78] H. Hakimova, S. Kim, K. Chu, S. K. Lee, B. Jeong, and D. Jeon, "Ultrasound stimulation inhibits recurrent seizures and

improves behavioral outcome in an experimental model of mesial temporal lobe epilepsy," *Epilepsy Behav.*, vol. 49, pp. 26–32, Aug. 2015.

[79] D. W. Gulick, T. Li, J. A. Kleim, and B. C. Towe, "Comparison of Electrical and Ultrasound Neurostimulation in Rat Motor Cortex," *Ultrasound Med. Biol.*, vol. 43, no. 12, pp. 2824–2833, Dec. 2017.

[80] S.-S. Yoo, K. Jung, Y. Zhang, N. Mcdannold, A. Bystritsky, and F. A. Jolesz, "Non-invasive Suppression of Animal-model Chronic Epilepsy using Image-guided Focused Ultrasound," in *Magnetic Resonance in Medicine*, 2010, vol. 97, no. 2, pp. 2010–2010.

[81] W. J. Fry, V. J. Wulff, D. Tucker, and F. J. Fry, "Physical Factors Involved in Ultrasonically Induced Changes in Living Systems: I. Identification of Non-Temperature Effects," *J. Acoust. Soc. Am.*, vol. 22, no. 6, pp. 867–876, Nov. 1950.

[82] "24-well Plate with PEDOT Electrodes on Glass (24W300/30G-288) | www.multichannelsystems.com." [Online]. Available: https://www.multichannelsystems.com/products/24-well-plate-pedot-electrodes-glass-24w30030g-288. [Accessed: 12-Aug-2019].

[83] Philips, "Capacitive micromachined ultrasonic transducers | Philips Innovation Services." [Online]. Available: https://www.innovationservices.philips.com/looking-expertise/mems-micro-devices/mems-applications/capacitive-micromachined-ultrasonic-transducers-cmut/. [Accessed: 10-Jan-2019].